University of Dundee

University of Dundee

Reflective Coloration from Structural Plasmonic to Disordered Polarizonic

Assad, Mhd Adel; Homaeigohar, Shahin; Elbahri, Mady

Published in:
Advanced Photonics Research

DOI:
[10.1002/adpr.202100009](https://doi.org/10.1002/adpr.202100009)

Publication date:
2021

Document Version
Publisher's PDF, also known as Version of record

[Link to publication in Discovery Research Portal](#)

Download date: 29. May. 2021

Reflective Coloration from Structural Plasmonic to Disordered Polarizonic

Mhd Adel Assad, Shahin Homaeigohar, and Mady Elbahri*

The generation of pigment-free colors by nanostructures and subwavelength patterns has evolved in the last decade and outperformed the conventional paints in terms of durability, recyclability, and environmental friendliness. The recent progress in the field of structural coloration, particularly reflective coloration, offering a full-color gamut, has realized high-resolution printing, not attainable by the pigment paints. Herein, an overview of the various systems able to offer reflective coloration for a variety of optical applications with static and dynamic responses is presented. Specifically, an emphasis is given to recent works of the article's authors on the cooperative action of the disordered particles and dipoles that can generate specular reflective colors. In addition, further developments of reflective color nanosystems are discussed. In the first section, an overview of the recent progress in the field of plasmonic reflective structural coloration is provided. The second part of the article deals with the authors' latest findings with respect to polarizonic color generation and its implementation in various areas ranging from environmental detection and biosensing to colored solar perfect absorbers. The report is wrapped up with an outlook and summary.

1. Introduction

Colors and decorations are pivotal in the comprehension of our surrounding world and are the most ubiquitous facet of human visual perception. Billions of years ago, green algae and their derivatives had revoled the earth's surface from gray to green and revolutionized life's colors to as intriguing as we see them today. Ever since, living organisms have been widely benefitting from color for communication, self-defense, reproduction,

camouflage, among others. The remarkable diversity of colors, as seen in, e.g., the sapphire blue wings of the morpho butterfly, the thermochromic coloration of the chameleon, and the feathers of peacocks and ducks,[1] has drawn the attention of researchers for centuries.

In fact, colors are not originated only from pigments or dyes, but rather the interaction of light with the specific, unique, and self-assembled structures of living organisms bring about a variety of colors.[2] Inspired by nature, this concept has been the principle of structural photonic and plasmonic coloration based on periodic structures and diffraction grating while manipulating a reflection's vivid coloration, polarization, and the phase and intensity of the radiated light.

Lord Rayleigh, a British physicist, was one of the first scientists who studied structural colors to explain the blue hue of the sky based on light scattering by the molecules of the atmosphere.[3–6] Later, Gustov Mie developed the scattering model and thoroughly elaborated the colors of colloidal gold nanoparticles.[7] Such knowledge has enabled the tuning of the resonant properties[8–11] and facilitated further developments of structural colors of metallic nanostructures, as witnessed in the recent decade.[3,4,12–14] The plasmon of nanostructured materials is the quantized electron oscillations at the nanoscale dimensions. In this regard, plasmonic metasurfaces are an intriguing family of subwavelength architectures able to extraordinarily enhance and confine the optical fields with well-controlled intensity, phase, and polarization beyond the diffraction limit and are used in optical imaging,[15] macroscopic color holograms,[16–19] color filters,[20–26] and polarizers.[27]

Over the last few years, subwavelength isolated metal nanostructures and ultrafine plasmonic nanoparticles have drawn the attention of the research community as promising designs for color generation.[28–31] However, looking at the historical variety of the man-made plasmonic objects such as the old colorful mask of Tutankhamun, painted tiles, and the Roman Lycurgus cup (**Figure 1**), a collection of plasmonic colors, yet not vivid, is discovered.

Absorption and scattering have always been attracting researchers when studying plasmonic nanostructures, nanoparticles, and nanocomposites, whereas reflection has been rarely addressed. This might stem historically from our lack of perception of these nanomaterials in their reflection mode, where stained glasses composed of spatially disordered Au, Ag, or

M. A. Assad, Prof. M. Elbahri
Nanochemistry and Nanoengineering
Department of Chemistry and Materials Science
School of Chemical Engineering
Aalto University
02150 Espoo, Finland
E-mail: Mady.elbahri@aalto.fi

Dr. S. Homaeigohar
School of Science & Engineering
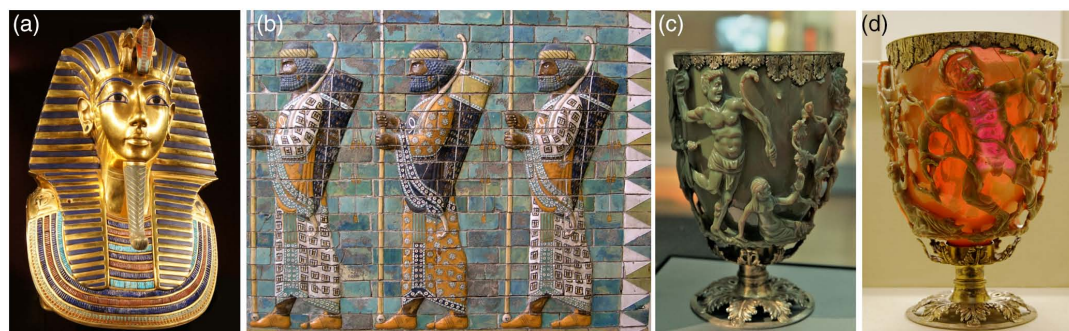University of Dundee
Dundee DD1 4HN, UK

Figure 1. Historical objects containing plasmonic nanocomposites. a) Mask of Tutankhamun. b) Tiles of the Palace of Darius, Susa, showing the Susian guards. b) Reproduced under the terms of a CC BY 2.0 license. The Lycurgus cup, both in (c) reflection mode and (d) transmission mode. d) Reproduced under the terms of a CC-BY 2.5 license.

Cu nanoparticles embedded in a dielectric matrix demonstrate unique colors when observed through transmission/ scattering, and a pale gray/green color via reflection (**Figure 2**). Yet, when placed under specific conditions to eliminate transmission and to diminish diffusive scattering such nanocomposites display vivid specular reflections arising from the disordered plasmonic and dipolar media, as seen in the lusterware shown in **Figure 3**, thus challenging the main conception that requires the existence of an even and mirror-like surface. This purely geometrical assumption not only neglects the illuminated matter but also opposes the electromagnetic dipole radiation concept that is well recognized by several scientists.[32–34]

The generation of vivid reflective colors is not achievable by the absolute suppression of reflection; rather it is preconditioned by the appearance of the "rest" reflection spectrum, as observed in the lusterware remains from 9th century Mesopotamia[35] (Figure 3). Upon visible light illumination, the lusterware demonstrates color changes based on the observation angle. The vivid

reflective colors derived from the luster are based on the reflection and interference effects emerging from ultrafine disordered nanoclusters with irregular size and spatial arrangement.[36] Such shiny colors that arise from a disordered nanosystem have been explained neither by the diverse existing plasmonic theories nor by the work of Gustav Mie proposed for metal nanoclusters, which is still in use today. In our opinion, such glossy colors emerging from the disordered nanosystems contradict the common knowledge of the artificial plasmonic dipole absorbers that are represented as dilute blackbody nanoheaters with the colors arising from the energy dissipation along with the blackbody radiation (Planck's law) of the oscillating charged particles and quantized dipoles. It should be borne in mind that this would be most possibly valid only when the extinction and/or electronic transition is contemplated as the single origin of color. Thus, the lusters of Mesopotamia shed light on the duality of colors (i.e., absorption/scattering vs reflection) and unravel the mystery of coloration by disordered nanoclusters. Recently, we challenged this general knowledge and provided a novel understanding by exploring *polarizonic resonance* with the specular reflection-based colors of disordered plasmonic nanoclusters and nanocomposites, and artificial plasmonic molecules among other radiating dipoles.[31,36–40] Indeed, the polarizonic colors emerging from such glassy and amorphous nanostructures could be of paramount technological importance for energy harvesting, biodetection, and aesthetics.

In this Review, we provide an updated overview of the field of structural reflective coloration based on the plasmonic and the new polarizonic reflective coloration systems with diverse ordered/disordered geometries. The color generated by such systems is represented by only a reflection peak. Correspondingly, reflective devices are devised and examined in the static and dynamic modes for various optical applications. Regarding the plasmonic structured colors represented by transmission and reflection dips, we refer the readers to our previous Review.[41]

In the first section, plasmonic nanostructures developed for various optical applications depending on the static reflective coloration mode are introduced. This part will be followed by the dynamic reflective coloration concept as the second section. The recently developed polarizonic concept is introduced and highlighted in the third section. Emphasis is given to the
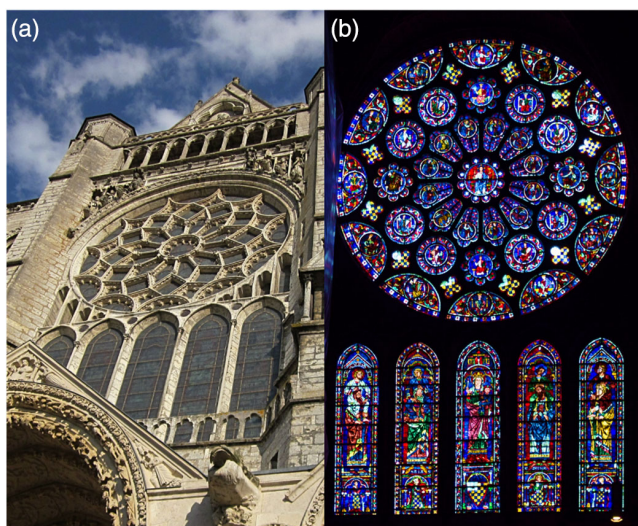

Figure 2. Photographic images of the Chartres Cathedral, France. a) The exterior image shows the stained glass in the reflection mode. b) The interior image exhibits vivid coloration of the stained glass through the transmission mode.
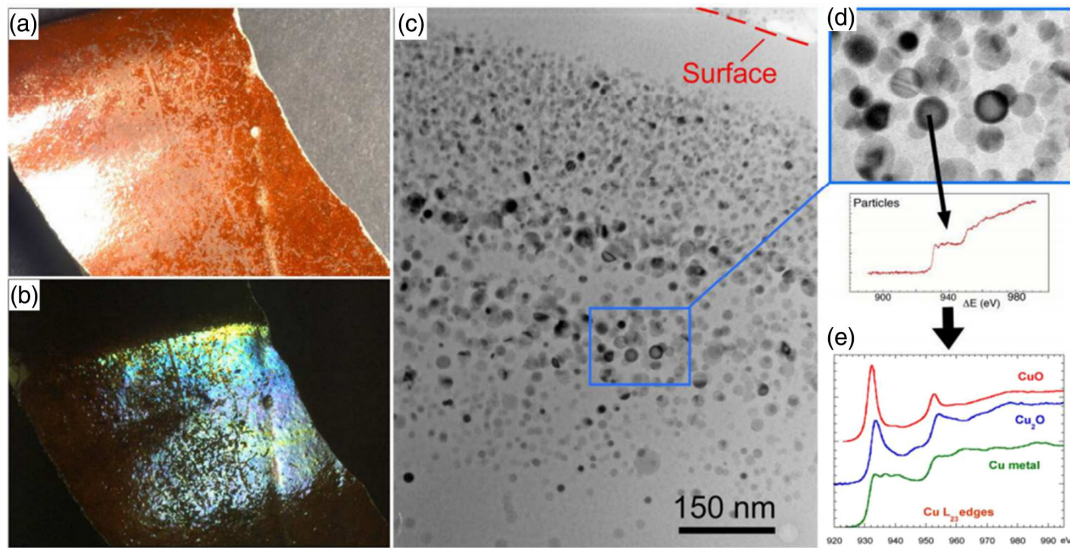
Figure 3. A lusterware found in Mesopotamia belonging to the 9th century CE. a,b) The photographs show the angle dependency as the specular reflection shifts from red (a) to blue/green (b). c,d) The particle distribution is shown via transmission electron microscopy (TEM) images. e) The chemical composition of the copper nanoparticles is verified by electron energy loss spectroscopy (EELS) graphs. Reproduced under the CC BY 3.0 license.[35] Copyright 2012, The Author, published by InTech Open.

polarizonic reflective coloration from disordered dipoles based on our recent works on artificial plasmonic dipoles and metal nanoparticles whose size is less than 10 nm and can generate colors via specular reflection. A highlight is presented for various optical applications operating based on far-field polarizonic radiation, including polarizability sensing, biosensing, decoration, perfect absorbers, and colored perfect absorbers. In this regard, the new concept of polarizonic interference along with the hybrid antireflection coating is discussed.

2. Structural Plasmonic with Static Coloration

So far, the creation of color has mostly been attributed to synthetic dyes and pigments, where they selectively absorb given wavelengths of incident light and allow the others to be reflected or transmitted. Yet, most of these pigments and dyes are carcinogenic,[42] nonbiodegradable,[43] nonenvironment friendly,[44] and suffer from many challenges, including color fading[45] and low resolution[46] (**Figure 4**).

In contrast, structural coloration that generates color based on the light interference of multilayered films or diffraction/scattering from periodic or aperiodic micro–nano structures is environmentally friendly and nontoxic. In addition, not only does it overcome the aforementioned challenges, but also it opens up new possibilities such as substitution of conventional paints (e.g., the commercial Lexus LC structural blue[47]) and industrial scalable high-resolution manufacturing (when combined with a roll-to-roll technique).

Due to their highly compact design, extraordinary resolution, and easy integration, plasmonic structural colors have gained wide interest in the areas of imaging, sensing, color displays, and digital cameras. In this regard, different plasmonic structures, such as nanoslits with periodical grooves,[48] metal–

insulator–metal stacks,[23,49] and annular aperture arrays[50,51] have been so designed to operate in the transmission mode.[52]

Here, we cover only the reflective coloration generated by periodic nanoantennas, plasmonic nanostructures, grating structures, and asymmetric Fabry–Perot cavities.

Plasmonic nanoparticles can be regarded as nanoantennas collecting and/or emitting visible radiation received from the far field at given frequencies.[53] To build up plasmonic color devices, the nanoantennas are arranged as micron-scale arrays called pixels. By varying the geometry, dimension, and patterned arrangement, the nanoantennas can induce customized localized surface plasmon resonances (LSPRs), and thus the desired reflection and transmission spectra.[52,54–57] Additionally, by using a predesigned plasmonic structure, they can further create an imaging pattern.[58,59]

Si et al.[52] elaborated the mechanism and theory behind the performance of a reflective plasmonic color filter consisting of silver nanorod arrays, shown in **Figure 5**a. The silver nanorods are arranged as arrays with periodicity (p) of 550 nm in x and y directions. They modeled every single nanorod via a dipole with polarizability of α, and the LSPR could be determined according to the coupling dipole theory.[60,61] Upon excitation of each resonator, a scattering field is radiated whose intensity depends on the resonator's dipole moment, whereas each resonator's static polarizability is determined through Equation (1)[62]

$$\alpha^{static} \propto V \frac{\varepsilon_m - \varepsilon_d}{3\varepsilon_m + 3\chi(\varepsilon_m - \varepsilon_d)} \tag{1}$$

where ε_m and ε_d are the relative permittivities of the metal and surrounding medium, respectively, χ is the geometrical factor that depends on the physical shape of the resonator (here, a nanorod), and V is the volume of a resonator. In case the entire nanorod array is considered infinite, the effective polarizability α^* of
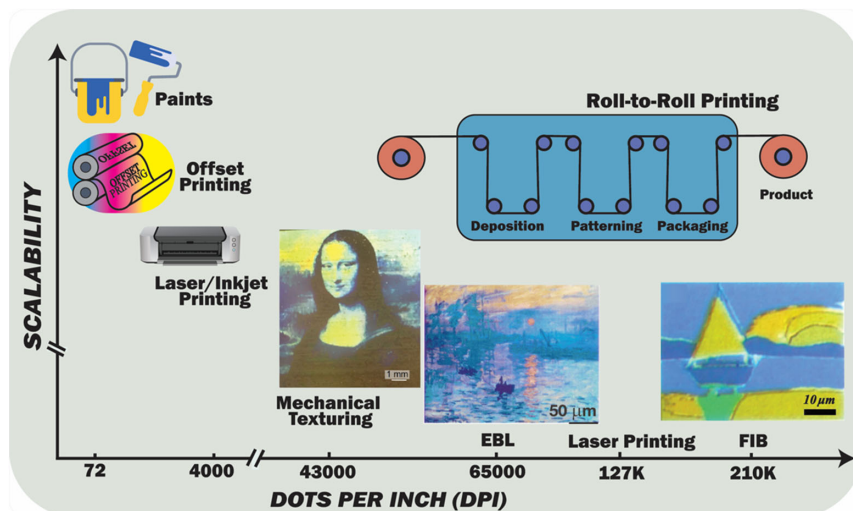
Figure 4. Figure of merit comparing pigments and dyes to structural colors. Paints, offset printing, and laser/inkjet printing are widely used and highly scalable in comparison to mechanical texturing,[134] EBL,[75] Laser printing,[69] and FIB patterning,[135] yet suffer from a 50-fold lower resolution. When EBL, FIB, or laser printing is combined with a roll-to-roll technique (top right), its scalability can be compared with that of pigments and dyes. Reproduction of Mona Lisa portrait via mechanical texturing reproduced with permission.[134] Copyright 2017, Elsevier B.V. Reproduction of Impression, Sunrise via EBL reproduced with permission.[75] Copyright 2014, American Chemical Society. Reproduction of pastel painting via FIB, reproduced under the terms of the CC BY license.[135] Copyright 2015, The Authors, published by Springer Nature.
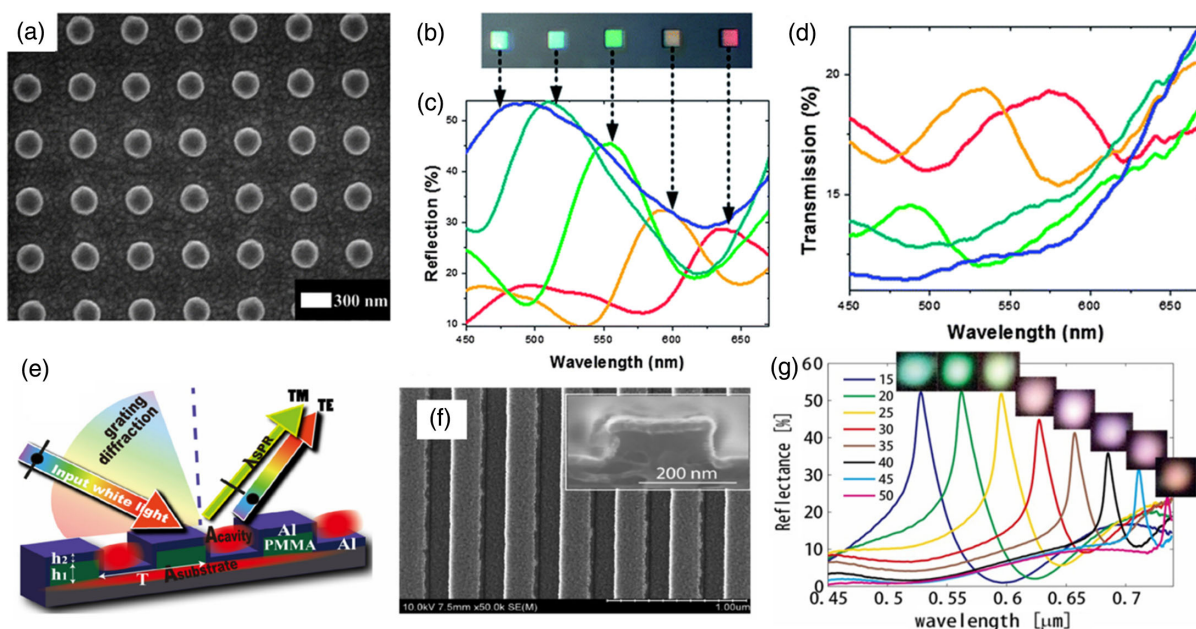
Figure 5. Plasmonic structures as reflective color filters. a) Top-view SEM image implies a silver nanorod array with periodicity (p) of 550 nm; b) Optical image showing the reflective colors emerged by different silver nanorod arrays (from left to right: $d/p = 0.938, 0.933, 0.930, 0.928$, and 0.926). The spectra showing different c) reflection peaks and d) transmission dips corresponding to different nanorod arrays. Reproduced with permission.[52] Copyright 2013, Royal Society of Chemistry. e) Schematic illustration of the reflective plasmonic color device based on an Al nanowire grating structure; f) SEM images of the grating structure with top and side views verifying that the Al layer has been conformally deposited on the dielectric reliefs of poly(methylmethacrylate) (PMMA). In this structure, the PMMA grating pitch (T) is 420 nm with a duty cycle of 50% and the thickness of dielectric (h_1) and Al (h_2) is 90 and 40 nm, respectively. The green arrow represents the lateral SPR-induced TM reflection peak with λ_{SPR}. The TM light with $\lambda < \lambda_{SPR}$ is diffracted whereas with $\lambda > \lambda_{SPR}$ it is absorbed by the nanocavities (A_{cavity}) and the Si substrate (A substrate). g) Angle-dependent reflection spectra and their corresponding color when the incident TM white light's angles vary from 15° to 50°. Reproduced with permission.[136] Copyright 2016, Optical Society of America.

**ADVANCED
SCIENCE NEWS**

www.advancedsciencenews.com

**ADVANCED
PHOTONICS
RESEARCH**
Open Access

www.adpr-journal.com

the LSPR on a single dipole resonator can be defined by Equation (2)[62]

$$\alpha^* = \frac{1}{\frac{1}{\alpha} - S} \tag{2}$$

where S is the array factor and engages the contribution of the other arrays. This factor for the square array with normal incidence can be estimated by Equation (3)[62]

$$S = \sum_{dipoles} e^{ikr} \left[\frac{(1 - ikr)(3cos^2\theta - 1)}{r^3} + \frac{k^2 \sin^2 \theta}{r} \right] \tag{3}$$

where θ and r refer to the dipole resonators' position. If $S = 1/\alpha$, the maximum effective polarizability occurs and results in a strong scattering. At the resonance, the backward wave scattering leads to a reflection peak (i.e., a dip in transmission).

The other main physical mechanism involved in plasmonic reflective coloration is based on guided-mode resonance (GMR) of planar dielectric waveguide grating.[63] The metallic gratings are promising structures for various optical applications due to their compact structure, outstanding spectral characteristics, and easy production. In this regard, a subwavelength metal (Al) nanowire grating structure on a Si substrate (Figure 5e,f) has shown the ability to generate a narrow monochromatic peak when reflecting visible p-polarized light. As shown in Figure 5g, the reflection wavelength depends on the incident

angle, giving rise to large color shifts. In this system, the monochromatic peak is caused by several factors, including the Fabry–Perot (F–P) absorption by the nanocavities at long wavelengths, significant diffraction at shorter wavelengths, and the surface plasmon resonance occurring at the Al–air interface.

The reflective plasmonic color could be also based on thin films of metal–dielectric multilayers acting with F–P cavity resonances.[64] The structure of this F–P resonator includes a lossless dielectric sandwiched between a partly reflective overlay metal nanostructured layer and a highly reflective mirror. The frequent round-trip phase delay of the light wave in the resonator brings about perfect absorption in F–P resonators.[65]

Yang et al.[64] developed F–P cavity–based reflective color filters comprising a nickel (Ni) thin (6 nm) film and an aluminum (Al) thick (100 nm) film, connected by a dielectric layer of silicon dioxide (SiO₂). Replacing the SiO₂ layer with an active ITO layer leads to the generation of reflective colors electrically (**Figure 6**a, middle). The Ni layer acts as a broadband absorber enabling the emergence of a wide range of highly saturated, vivid, and bright structural colors. The optical thickness of the SiO₂ layer controls the location of the absorption and reflectance peaks. Such a reflective color filter coupled with grayscale patterning techniques allows for high-resolution, high-contrast monolithic color printing. As shown in this study, high-resolution (over 50 000 dpi) full-color printing is accessible when using F–P-type elements as the pigments. In addition, such a reflective color filter exhibits angle insensitivity up to 60°. Due to the photonic
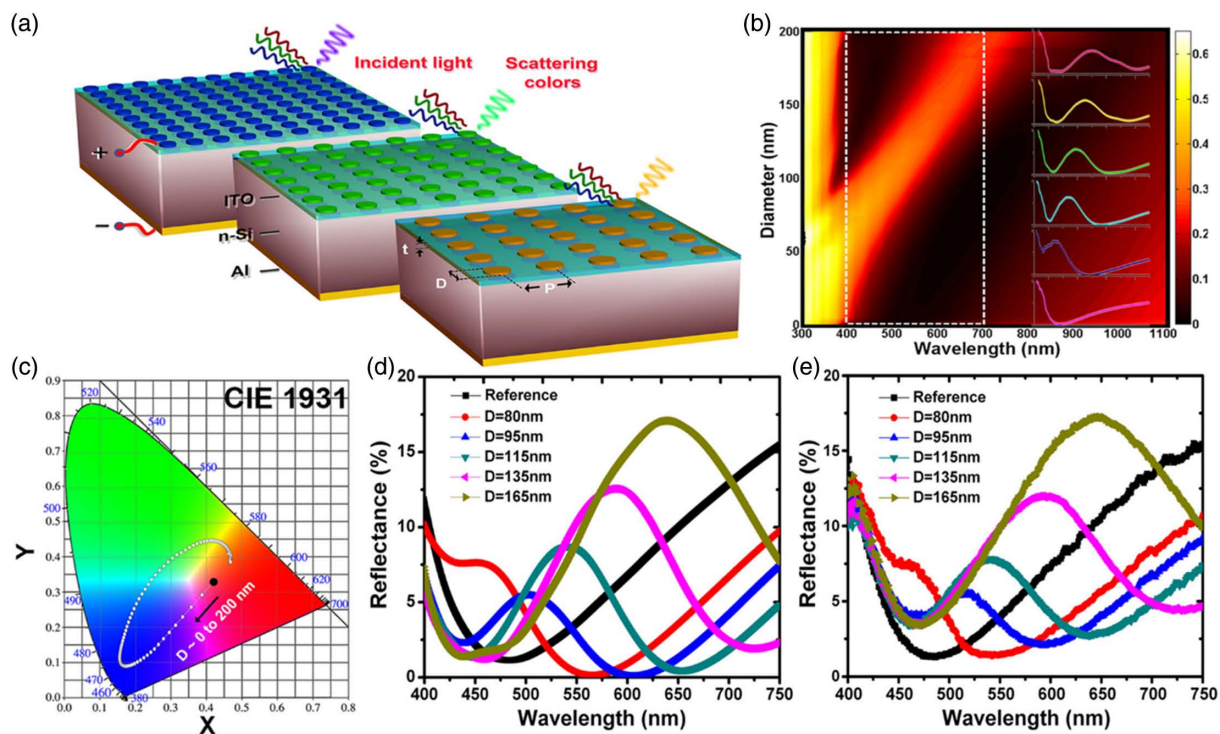
Figure 6. Plasmonic scattering coloration for optoelectronics. a) Schematic illustration of the Al nanodisk/ITO/n-Si/Al optoelectronic device. The Al nanodisks with a diameter of D are arranged periodically (P) in a square lattice. b) Contour plot of the reflectance versus the diameter of nanodisks ($D = 0$ to 200 nm and fill factor (F) = $D/P = 0.5$). c) CIE 1931xy chromaticity coordinates show the predicted colors with reflectance correlated to the spectra estimated in (b). d) The simulation and e) experimental reflection spectra of the color pixels containing Al nanodisks with diameters of 80, 95, 115, 135, and 165 nm and periods of 264, 296, 328, 360, and 392, respectively. Reproduced with permission.[137] Copyright 2016, American Chemical Society.

**ADVANCED
SCIENCE NEWS**

www.advancedsciencenews.com

**ADVANCED
PHOTONICS
RESEARCH**
Open Access

www.adpr-journal.com

action determined by the F–P dielectric cavity, once the condition of $\lambda = 2nd$ is fulfilled, the plasmonic reflective color emerges (Figure 6b,d,e). For such thick cavities, there is no need for ordered plasmonic nanostructures as a top layer and thus reflective colors can be realized even by random nanostructures, thus allowing for a variety of fabrication methods.[66]

Benefitting from the F–P interference effect, Yang et al.[67] developed a full-color printing concept based on a metal–dielectric–metal configuration. **Figure 7**a shows the structure of the interference color pixel comprising an ultrathin nickel top layer, a back reflector made of aluminum, and an intermediate oxide layer. Under white light illumination, such a structure offers a high reflective contrast and vivid colors that are generated by intensive destructive interference effects. The dielectric's thickness in each F–P cavity governs the pixel color, as shown in Figure 7b. Utilizing grayscale lithography, the tunability of the

filling factor and the thickness of the F–P cavity are realized. As a result, diverse colors with different adjustable brightness and saturation are generated.

Jiang et al.[68] suggested an efficient approach for plasmonic printing based on the creation of a layer of silver nanoparticle ink atop a nanostructured transparent polymer substrate. The as-formed silver layer can offer robust structural diffractive colors that are tunable by changing the geometries of the nanostructure. This technique enables a scalable and inexpensive printing method to produce a wide range of various structural colors with high resolution that could be used for regular publishing and display applications.

As schematically shown in **Figure 8**a, first, a nanostructured transparent substrate is made through an imprinting process by a premanufactured stamp onto a polyethylene terephthalate sheet. Subsequently, using inkjet printing, ink droplets, which
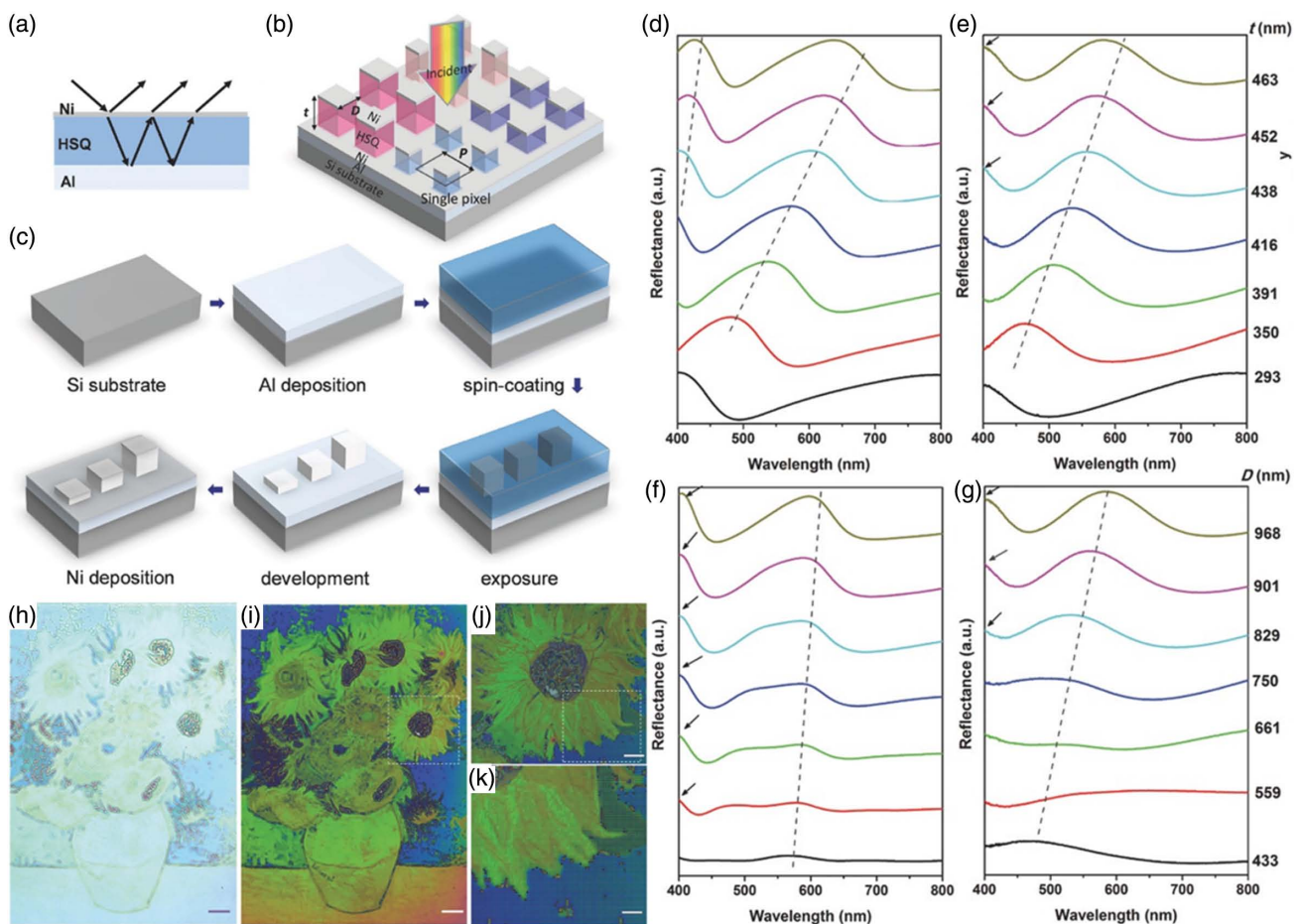

Figure 7. Grayscale patterned FP cavity based plasmonic reflective color printing. a) The fundamental structure of an interference color pixel based on metal–dielectric–metal FP resonance cavities. HSQ represents hydrogen silsesquioxane. b) Schematic illustration of the FP resonator–based monolithic full-color printing device. Each square pixel as large as P includes only one FP resonance cavity (thickness t and size D) and its Ni and Al metallic layers are as thick as 6 and 100 nm, respectively. c) The grayscale lithography of FP cavities with different thicknesses. d) Simulated and e) measured reflection spectra for the FP cavities with different t when the filling density is as large as 100%. f) Simulated and g) measured reflection spectra for FP cavities with various filling densities (when the square size D varies from 433 to 968 nm at a fixed t of 463 nm). The arrows in (e)–(g) stress the third-order interference modes of the studied FP cavities. Optical images of Van Gogh's sunflower painting h) before and i) after Ni deposition (scale bars: 50 μm). j) Magnified image of a selected region of the sunflower painting in (i), emphasizing its color uniformity (scale bar: 20 μm). k) Higher-magnification image of the marked square in (j) implies the resolved pixels with various colors caused by the interference effect (scale bar: 10 μm). Reproduced with permission.[67] Copyright 2017, John Wiley and Sons.
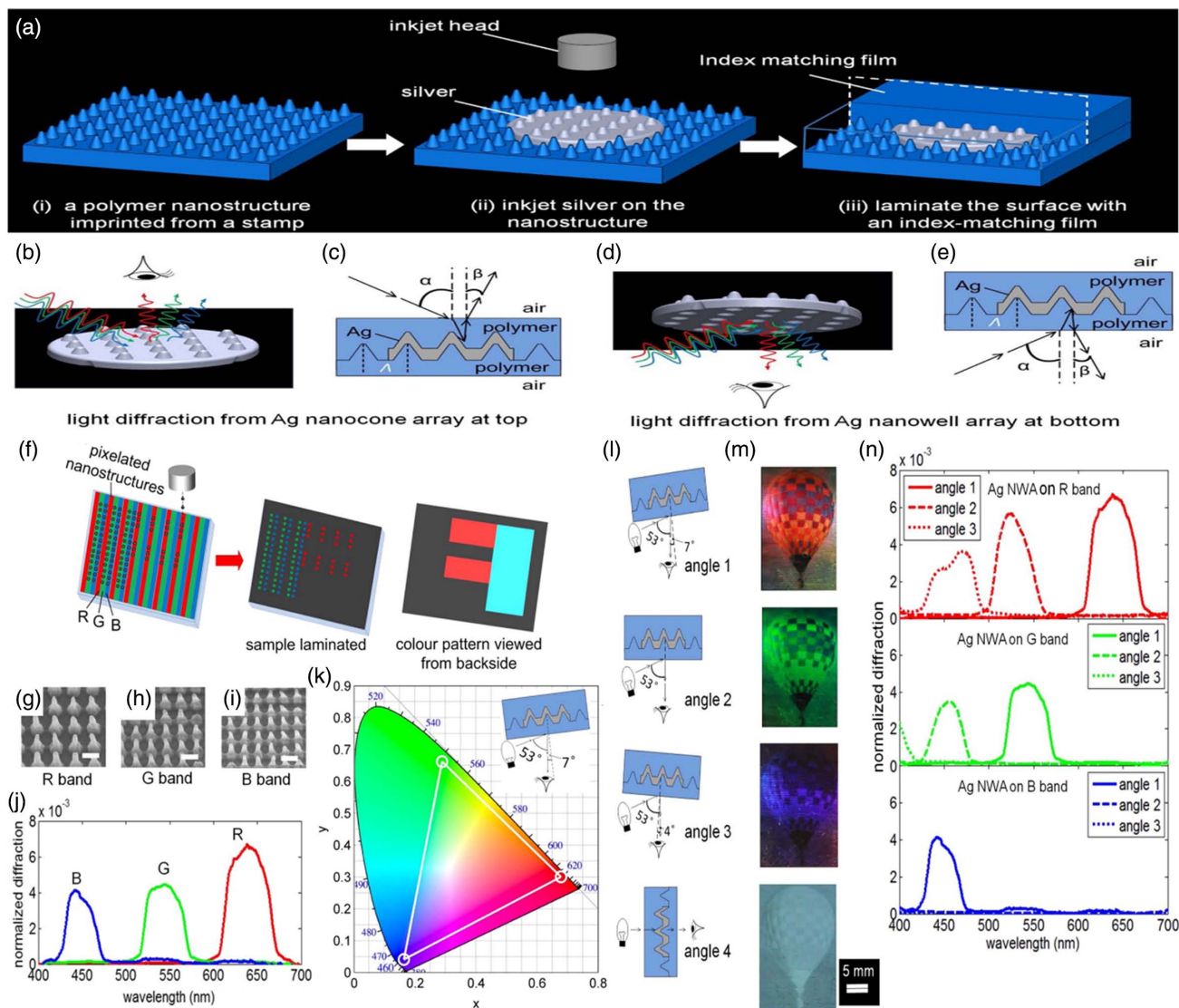
Figure 8. Ink-jetted Ag nanostructure for plasmonic diffractive color printing. a) Schematic illustration of the preparation process of the inkjet silver nanostructure. b,d) Schematic illustration of the diffractive colors observed from the Ag nanocone and nanowell arrays, respectively. c,e) Side-view schematic illustration of the diffraction of light by the nanocone and nanowell array perceived as diffractive colors from the top and back sides, respectively. f) Schematic illustration of the full-color printing process. The substrate surface consists of Ag pixelated nanostructures as periodically repeated R, G, and B pixel bands. For a specific color image, a digital pattern is made and then inkjet printed onto the pixel bands considering precise registration relative to the pixel layout. g–i) SEM images show the polymer nanostructures in R, G, and B pixel bands, respectively. The scale bar represents 500 nm. j) The diffraction spectra of the silver nanowell arrays on R, G, and B bands. k) CIE-1931 chromaticity map of the diffractive colors of three printed silver nanowell arrays. The circled areas represent the colors of the silver nanowell arrays, and the triangle encompasses the range of colors that can be mixed from the three silver nanowell arrays. l) Schematic illustration of the different lighting modes and viewing angles. m) Camera images of a printed image of a hot air balloon taken at the different angles defined in (l). n) Angle-sensitive diffraction spectra of the silver nanowell arrays on R, G, and B bands measured at the angles defined in (l). Reproduced with permission.[68] Copyright 2016, American Chemical Society.

contain silver nanoparticles, are printed on top of the nanostructured substrate designed according to a customized pattern. As the silver ink dries, it turns into a solid silver thin film molded by the polymer nanostructured substrate. The as-molded silver nanostructure can generate diffractive structural colors that can be tuned by the shapes and geometries of the diffractive nanostructures along with the viscosity of the silver nanoparticle–containing ink. Subsequent to printing, the whole surface is coated

with an impedance-matching layer to maintain a transparent background and to protect the silver from exposure to the ambient environment.

To address insufficient resolution and low scalability of plasmonic color prints, Kumar et al.[69] encoded color information in the structural (dimensional) details of plasmonic nanostructures to enable tailoring their plasmon resonance and thus the individual pixels' colors. They enhanced the scattering intensity of the

ADVANCED
SCIENCE NEWS

www.advancedsciencenews.com

ADVANCED
PHOTONICS
RESEARCH
Open Access

www.adpr-journal.com

particle resonators made of silver (15 nm) capped by gold (5 nm) by depositing them atop a metal back reflector to create 250 nm pitch pixels reflecting individual colors independent of their periodicity. Particularly, the back reflector acts as a mirror, enhancing the scattering intensity of the resonators. Furthermore, the larger Ag/Au disks offer stronger resonance peaks due to their increased scattering strength. A resonance dip is induced due to the power absorption by both the smaller resonators and slightly the back reflector. As a result of the interference occurring between the surface modes and broad resonance of these nanodisks and nanoholes (i.e., Fano resonance), narrower spectral peaks emerge and thus purer colors. Accordingly, bright-field reflective color prints with high resolutions up to the optical diffraction limit (and as high as 100 000 dpi) were obtained. Moreover, this technique allows for large-scale color printing via nanoimprint lithography, thus offering potential in the production of microimages for nanoscale optical filters, steganography, and optical data storage.

Mudachathi and Tanaka[70] have developed a simple yet operative color printing technique based on submicrometer-scale plasmonic pixels. Such pixels made of Al, as large as 260 nm (i.e., slightly over the optical diffraction limit), enabled near-perfect light absorption of two distinct wavelengths, leading to the generation of saturated colors. This technique cannot confer a resolution as high as that offered by the fine nanostructured pixel-based techniques (i.e., near diffraction limit), which is not necessary for various applications such as consumer product coloration. However, it facilitates large-scale production through a single-layer fabrication process using electron beam lithography (EBL) and thermal evaporative metal deposition.

Similarly, Rezaei et al.[71] have targeted the costly nature of plasmonic color printing for large-scale images due to the need for specific patterning methods of nanostructured pixels such as EBL and focused ion beam (FIB) that are complicated and lengthy. They developed a novel printing technique for structural diffractive color images based on a reusable generic nanosubstrate with red, green, blue, and infrared subpixels. The nanosubstrate is covered by a mask layer, subsequently patterned according to the desired color image. The patterning creates size-controlled apertures and thereby enables selective imprinting of subpixels of the nanosubstrate onto a second polymeric substrate. The colors needed depending on the image (i.e., the pattern created on the mask layer) are obtained by adjusting the active area of the subpixels controlled by the aperture sizes. For instance, a yellow pixel is obtained by exposing the red and green subpixels and covering the blue and infrared subpixels. The patterning of the mask layer takes place by laser lithography with a submicron resolution. The nanosubstrate can be cleaned and used several times for printing various images. Accordingly, the fabrication cost and throughput are superior to conventional photolithography. However, as the authors declared, the printing resolution could be maximally up to 25 400 dpi, which is much lower than that obtained by the EBL nanostructures with 100 000 dpi resolution. The suggested technique can be used for both optical data storage and document security along with publicity applications such as posters, magazines, newspapers, and book covers.

Xue et al.[72] have researched the scalability of plasmonic reflective color printing based on a novel approach consisting of a plasmonic broadband absorber (PBA) along with a conjugate twin phase modulation (CTPM). This technique not only enables scalable, full-color printing but also provides the ability to reverse color transformations. Such a possibility could be applied in constructing functionalized prints for security and storage. The CTPM can enlarge the peak–valley (p–v) ratio of reflection spectra, and thus provide high saturation of the emerged colors, and the PBA, i.e., a metal (silver) island film, narrows the reflective peaks. Accordingly, this supplementary function leads to the generation of vivid full reflective colors. As shown in **Figure 9**a, the plasmonic prints are manufactured based on an electrochemically grown anodic alumina (AAO) template and a sputtered silver island film, which assure a scalable, inexpensive production method (up to the centimeter scale) that is much less complicated than EBL. In such a structure, when the average thickness of the silver layer increases, a silver island film is constructed which can notably raise the p–v ratios in the reflection spectra (Figure 9b), leading to the emergence of a vivid pink color. By filling the pores of the AAO with different dielectrics (e.g., ethanol, toluene) the n_P can be adjusted, and the generated colors are manipulated in a controlled manner (Figure 9e). As soon as the filling solution evaporates, the color returns to its former state.

As mentioned before, generation of highly saturated and bright structural colors is not easy and necessitates the fabrication of very small nanostructures.[73,74] To address such challenges, one advanced solution could be utilization of metal–insulator–metal (MIM) structures. Wang et al.[73] fabricated MIM nanodisks that fortify the enhanced in-phase electric dipoles, thereby shifting them to a shorter wavelength when compared to a singular disk. **Figure 10**a schematically illustrates a tandem nanodisk square array on a SiO$_2$ substrate. The hybridization between Wood's anomaly and the enhanced in-phase electric dipole mode of the nanodisk pairs leads to the appearance of narrow and high-resonance reflection peaks and deep transmission dips (Figure 10b–e). As shown in Figure 10f, the emerged colors depend on the periodicity and radius of the nanodisk. Adjusting the periodicity of the array and/or the radius of the involved nanodisks enables the generation of full colors, as represented by a CIE1931 chromaticity map shown in Figure 10i–l. The technique developed can potentially be used in imaging, storage, display, and sensing.

Miyata et al.[74] developed an MIM device based on aluminum gap-plasmonic nanoantennas. They could manifest that the properties of an individual antenna encompassing intensive absorption at dual dissimilar frequencies can be encoded into a singular pixel. Moreover, the basis of this approach is the reality that these nanostructures offer strong resonances due to the metallic nanogap, in which light is confined. The applicability of the MIM-based color pixels for subwavelength printing was validated by displaying colorful microscopic letters. The coloration was omnidirectional, polarization-independent, and notably durable. Given the cost-effectiveness and high stability of aluminum, the suggested approach could be beneficial in printing microimages for security purposes, or for data storage. It is noteworthy that aluminum suffers from a high loss leading to a low Q-factor, thus lowering the color variety in the plasmonic printing.[74,75]
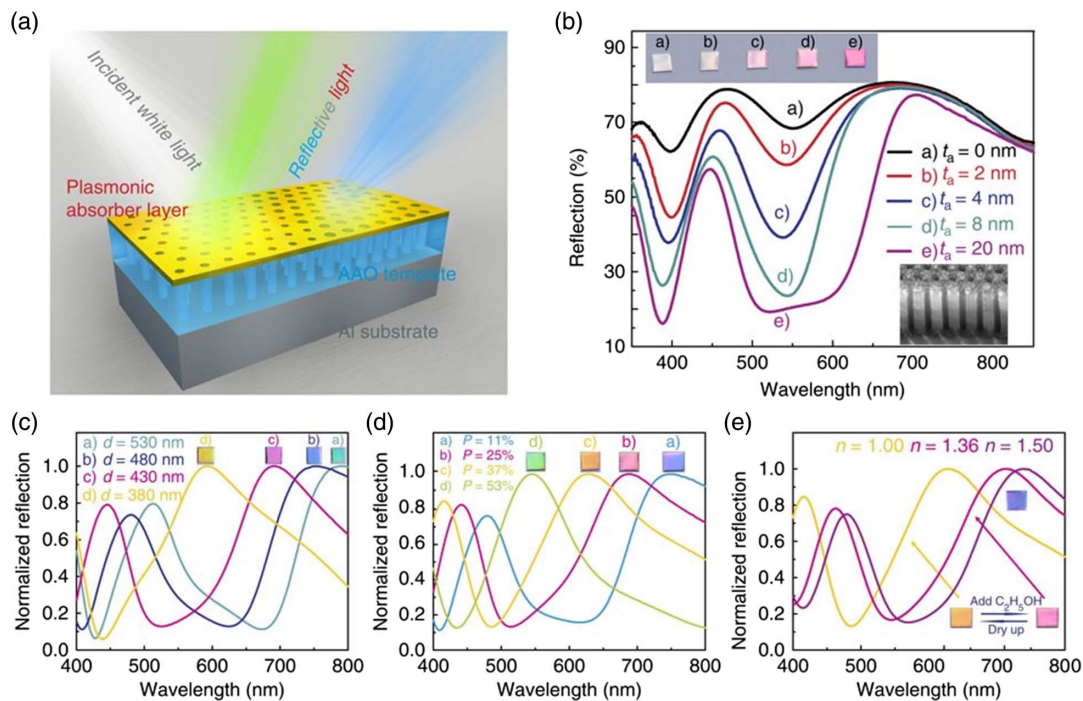
www.advancedsciencenews.com

ADVANCED
PHOTONICS
RESEARCH
Open Access
www.adpr-journal.com

Figure 9. Scalable, full-color plasmonic reflective color printing. a) Schematic illustration of the CTPM–PBA device wherein the top layer is a PBA layer, the middle one an AAO template, and the bottom one an Al substrate. b) Reflective spectra of the CTPM–PBA device versus Ag sputtering time, t_s. The camera images are related to the measured samples ($4 \times 4 \, mm^2$). In addition, the SEM image (scale bar, 200 nm) shows the morphology of the sample ($t_a = 20 \, nm$) under a tilted angle of $45°$. c) Reflective spectra of the CTPM–PBA device based on AAO with different thicknesses, d. The samples with longer t_o possess a larger d, which induces a shift for the reflective peak. d) Reflective spectra of the CTPM–PBA device ($d = 480 \, nm$) with different porosities, P. A longer t_e increases P, and decreases the average refractive index, thus blueshifting the reflective peak. e) Reflective spectra of the CTPM–PBA device ($d = 480 \, nm$, $P = 37\%$) under different conditions. Reproduced under the terms of the CC BY license.[72] Copyright 2015, The Authors, published by Springer Nature.

3. Dynamic Plasmonic Reflective Coloration

One important bottleneck of the mentioned plasmonic reflecting systems is that the plasmonic nanostructures perform as passive/static devices offering consistent outputs under the same inputs conditions. This feature notably restricts their applicability because of the need for further investments to design and fabricate another similar device able to offer a slightly changed output. Therefore, dynamic, active plasmonic systems are highly demanded. Such devices mainly consist of a reconfigurable property induced by certain external stimuli. This part discusses the most recent developments in this area that promise attractive opportunities for plasmonic research in the future.

Utilizing the fascinating feature of structured plasmonic metamaterials in tuning optical resonance, and thus plasmonic color, via change of composition, Wang et al.[76] developed highly ordered Au/Ag nanodomes as dynamic plasmonic nanostructures. They could devise a biomimetic mechanical "chameleon" that functioned by varying the Au/Ag core–shell structures, enabling plasmonic modulation through an electrodepositing/stripping process. The coating process is performed in an electrochemical cell dynamically and depending on the applied voltage the silver ions are either deposited onto or stripped from the gold nanodomes. This approach allows for real-time light manipulation in compliance with the color details of any given surrounding medium.

Figure 11a shows the reflection spectra of the structure versus Ag deposition time. The longer is the deposition time, the more the reflection peak blueshifts. The reflection's peak positions versus depositing/stripping time are shown in Figure 11b, where the inset images show the generated colors for the points nominated. Figure 11c indicates a chromatic map of the structure based on the points extracted from Figure 11a that further proves the achievement of an alterable nearly full-color development via a plasmonic cell. Figure 11h schematically illustrates the mechanical chameleon fabricated in this study whose body is enclosed with color patches that comprise the plasmonic cells. The mechanical chameleon is equipped with fine color detectors able to identify the details of the surrounding area. The received data are then analyzed and transferred to the color patches, thereby changing the mechanical chameleon's color. Figure 11j shows the chameleon moving in different successive times in front of a triple-color scene.

As already discussed, plasmonic color printing by metasurfaces has bloomed the color display research, thanks to an extraordinary subwavelength resolution and compact optical data storage. In this regard, there is still a need for advanced dynamic plasmonic-based displays exhibiting dynamic multicolor animations along with highly secure encryption. Duan et al.[77] developed catalytic magnesium-based metasurfaces that meet the mentioned needs as dynamic displays. In the plasmonic device,
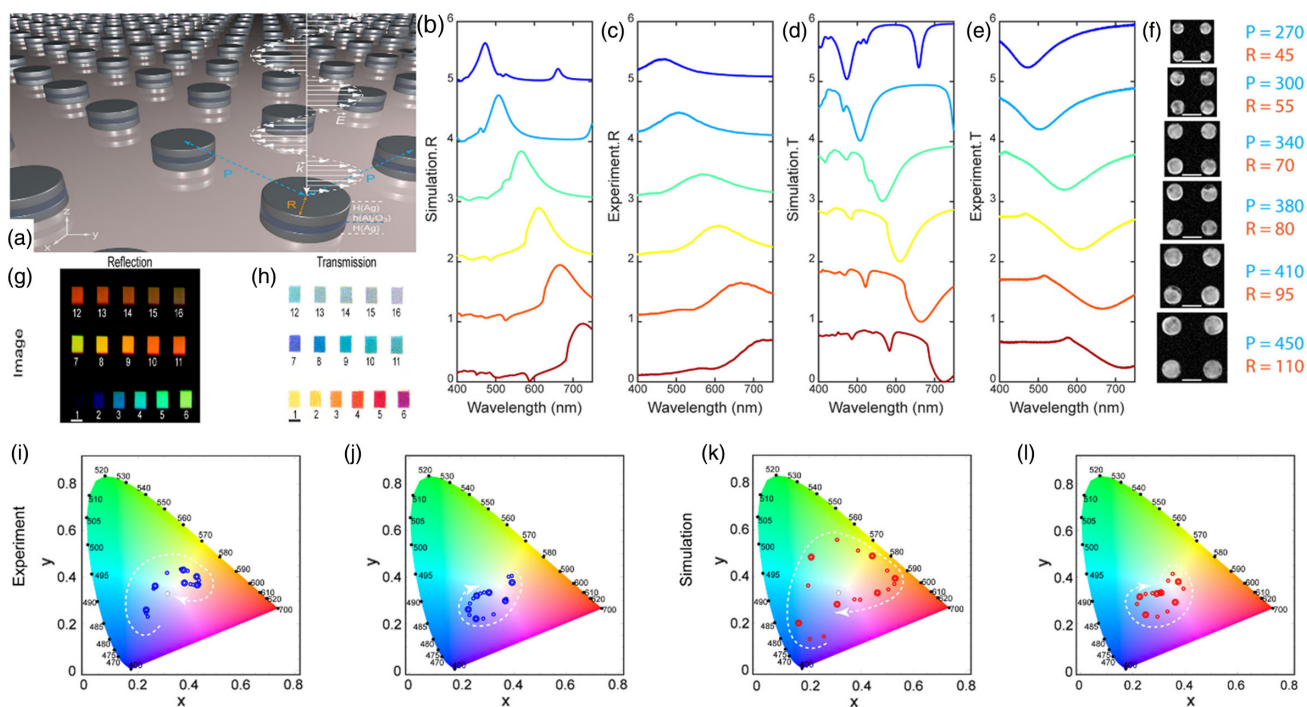
**ADVANCED
SCIENCE NEWS**

www.advancedsciencenews.com

**ADVANCED
PHOTONICS
RESEARCH**

Open Access

www.adpr-journal.com

Figure 10. Reflective and transmissive coloration by MIM structures. a) Schematic illustration of the tandem nanodisk square array. In this schematic, the array's structure is specified with period P, radius R, and thickness of the Ag layers H and the Al_2O_3 layer h and is illuminated at normal incidence with y-polarized white light. b) Simulated and c) experimental reflection spectra; d) Simulated and e) experimental transmission spectra. f) The SEM images of the array structures whose reflection and transmission properties are exhibited in (b–e). The period and radius values of the array structures are indicated on the right. Scale bar: 200 nm. The generated g) reflection (from dark blue to red) and h) transmission (from yellow to cyan) colors for 16 samples. Scale bar: 40 μm. The CIE1931 chromaticity space including i,j) experimental and k,l) simulated colors. The six colors of (b–e) are specifically shown by double rings. The white dashed arrows imply the evolution trend for the colors corresponding to the increase of the radius and period. Reproduced with permission.[73] Copyright 2017, American Chemical Society.

the dynamic pixels consisted of Mg nanoparticles placed between capping layers of titanium Ti/Pd. As schematically shown in **Figure 12**a, the introduction of hydrogen and its absence in the magnesium nanoparticle–based dynamic pixels enabled plasmonic color printing, erasing, and tuning.

The possibility of tuning, erasing, and restoring plasmonic colors[78,79] can be beneficial in the development of high-quality color-tunable plasmonic microprints. Duan et al.[77] demonstrated this applicability by creation of a microprint based logo, as shown in Figure 12d. By exposure to hydrogen, the logo experiences a dynamic color change. Up to 23 s, the color changes abruptly; afterward the logo starts fading and completely vanishes after 566 s. In contrast, after exposure to oxygen, the logo's colors are restored, and no significant color change is seen after 2224 s. In addition to the aforementioned utilities, using various dynamic pixels with different color transformation kinetics, plasmonic animations are realized (Figure 12e). Also, information can be encoded on specific pixels that are not detectable either by optical microscopy or by scanning electron microscopy but can be revealed using hydrogen as a deciphering key. This possibility could be utilized for encryption and anticounterfeiting applications.

A combination of photoswitchable molecules[40,79,80] and plasmonic nanostructures could lead to new opportunities in the field of optics, including display technologies. For instance, reflective electronic papers are highly demanded thanks to their lower energy consumption and pleasant visibility under ambient light.[81] However, the technologies that can offer reflective color displays are relatively few. In this regard, conjugated polymers are a promising candidate, yet their electrochromic property suffers from high switching times, poor optical contrast, and low coloration efficiency.[82] Despite such shortcomings, when coupled with plasmonic nanostructures, conjugated polymers can offer adjustable absorption, thus tuning the optical activity.[83,84] The plasmonic nanostructured systems studied so far are mainly based on nanoparticles and rely on the modulation of transmission. In an innovative attempt, Xiong et al.[85] have demonstrated a plasmonic nanostructure generating reflective colors that can be electrically modulated by a conjugated polymer. The developed material can be used as a flexible screen. The optical absorption of a conjugated polymer is electrically controlled to tailor the reflection of the ultrathin plasmonic nanostructure. This approach enables high polarization-independent reflection (>90% in air) and brings about optimum contrast (30–50%), low response times (milliseconds), negligible power consumption (<0.5 mW cm^{-2}), and long-term durability. Interestingly, the plasmonic metasurfaces possessing the red–green–blue (RGB)-related pixels offer reflectivity and contrast comparable to those of the printed ink. Eventually, as shown by Xiong et al. the RGB pixels can generate secondary colors and images that are switched on/off.
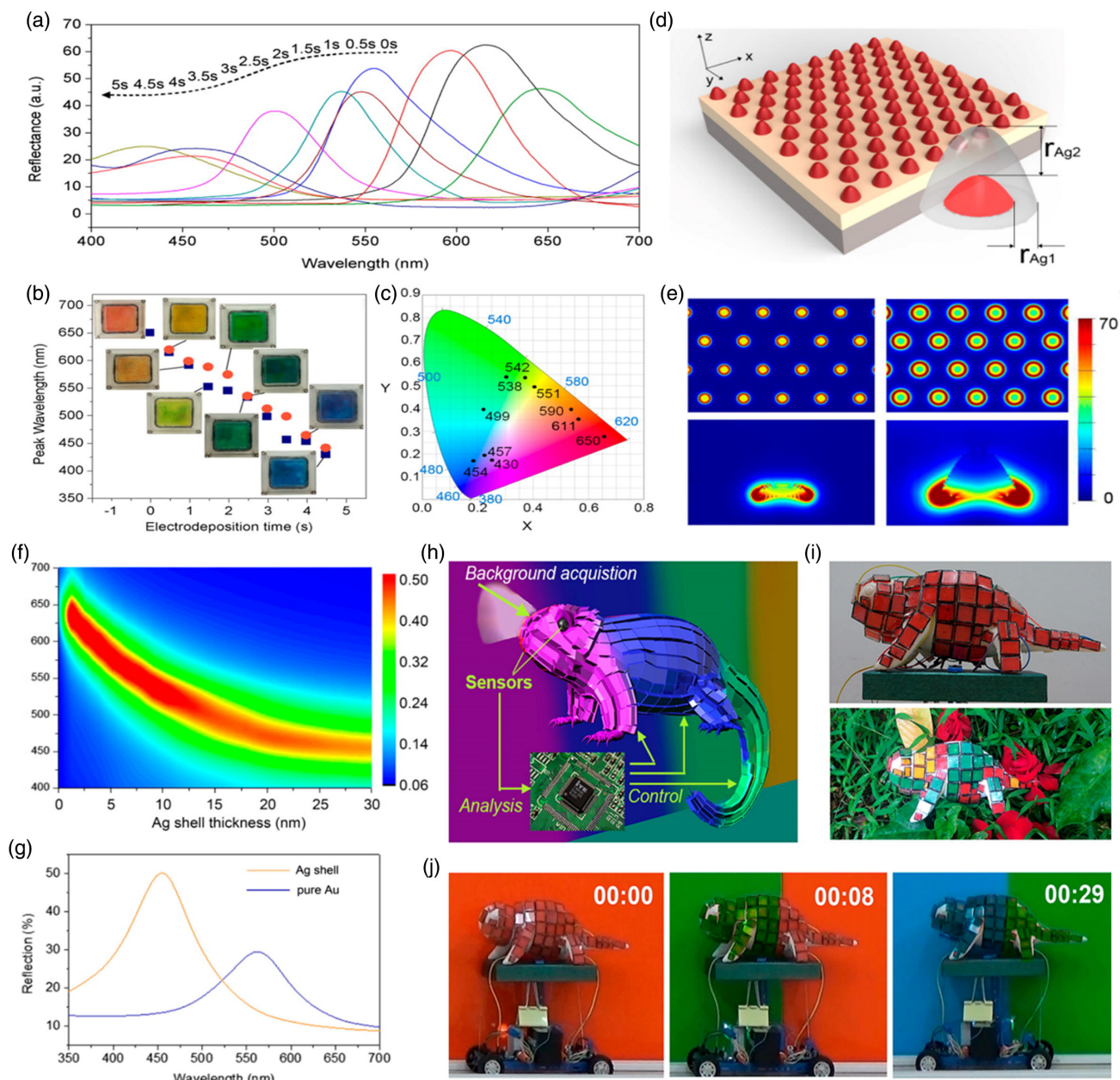
**ADVANCED
SCIENCE NEWS**

www.advancedsciencenews.com

**ADVANCED
PHOTONICS
RESEARCH**
Open Access

www.adpr-journal.com

Figure 11. Active camouflage by dynamic reflective coloration. a) Reflection spectra of the bimetallic structure after different electrodeposition times. b) Shift of the reflection peak wavelength depending on electrodepositing (blue squares) and electrostripping times (orange dots). Insets are camera images of the plasmonic cells related to the selected points. c) CIE map of the plasmonic cell. d) Schematic illustration of the simulation model. e) 2D reflection spectra versus Ag shell thickness. f) Simulated electric field distribution for Au nanodomes at 650 nm light (left) and Au/Ag shell (thickness of 30 nm) at 450 nm (right). g) Reflection spectra of the Ag (30 nm)/Au core–shell nanodome (orange curve) and the Au nanodome (blue curve) with equal size and shape. h) Schematic illustration of the mechanical chameleon covered with plasmonic cells. i) Top row: camera image of the red-state mechanical chameleon. Bottom row: camera image of the chameleon on grass. j) Screenshot of the change of the plasmonic color of the chameleon while moving in front of scenes in various colors. Reproduced with permission.[76] Copyright 2016, American Chemical Society.

To enable on/off switching of colors, conjugated polymers with tunable optical absorption were used. As shown in **Figure 13**g, by applying a voltage of +0.57 V to a solution containing sodium dodecylbenzenesulfonate and pyrrole, doped polypyrrole films were electropolymerized on a plasmonic metasurface. Accordingly, as shown in Figure 13f, the adjustment of the reflections of RGB samples with high contrast could be realized.

Altering the periodic structure and/or refractive index is the principle of tuning optical properties in a dynamic photonic system.[86–88] Such systems enable optical responsiveness, thereby operating as optical transducers able to detect external stimuli.[89,90] In this regard, Yetisen et al.[91] developed a diffractive optical sensor utilizing a nanocomposite comprising periodic diffraction gratings of Ag nanoparticles embedded in a hydrogel
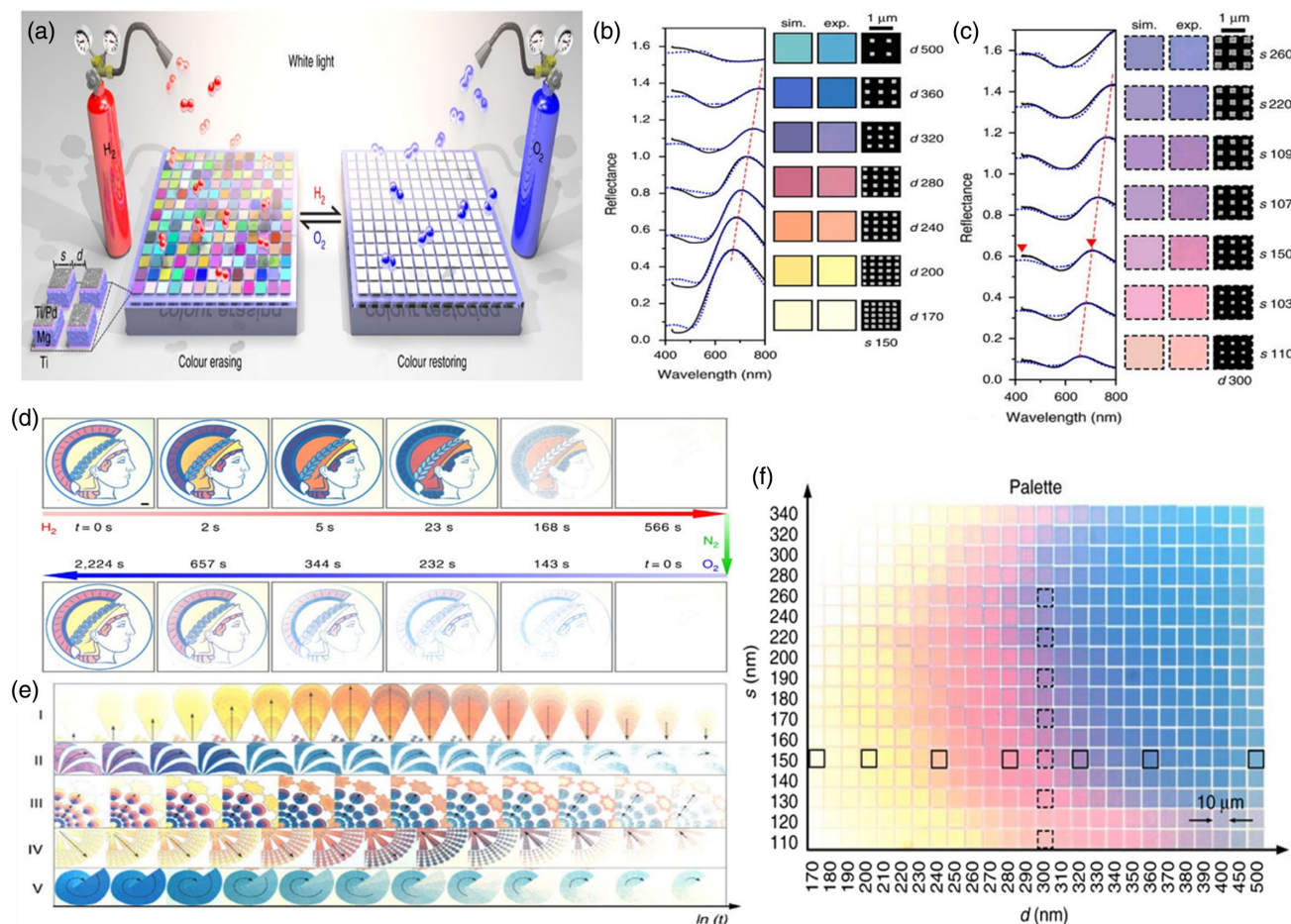
ADVANCED
SCIENCE NEWS

www.advancedsciencenews.com

ADVANCED
PHOTONICS
RESEARCH
Open Access

www.adpr-journal.com

Figure 12. Advanced plasmonic displays by dynamic reflective coloration. a) Schematic illustration of the plasmonic metasurface based on Mg nanoparticles (sandwiched between Ti/Pd capping layers and a Ti adhesion layer) illuminated with incident unpolarized white light. Each color square (10 μm) contains Mg nanoparticles arranged in a lattice with a period of $s + d$ in both directions. s and d are the sizes of the square-shaped particles and the interparticle distance, respectively. As shown here, the colors of the plasmonic metasurface can be erased or restored upon hydrogen or oxygen exposure through reversible phase transition from Mg to MgH$_2$, respectively. b,c) Experimental (black) and simulated (blue-dotted) reflectance spectra of the selected color squares from the color palette shown in (f) along with the corresponding SEM images of the pixels. The red dashed line implies the reflectance peak shift. d) Optical micrographs of the Minerva logo of the Max-Planck Society undergoing color erasing and restoring during hydrogenation and dehydrogenation cycle, respectively. Scale bar: 20 μm. e) Snapshots of the firework animations created by dynamic plasmonic effects over time. f) Color palette made via controlled tuning of s and d. Reproduced under the terms of the CC BY license.[77] Copyright 2017, The Authors, published by Springer Nature.

based on polyhydroxyethyl methacrylate (pHEMA). In this system, thanks to the vertical periodicity, the diffracted light's spectrum is highly narrowed to generate a given color. As the authors state, by using 6 ns pulsed standing waves ($\lambda = 532$ nm) at 240 mJ, the Ag nanoparticles (as small as 13 ± 9 nm in diameter) were arranged into domains with a periodicity of half of the wavelength, as shown in **Figure 14**d. The as-formed hologram performs as a sensor when its diffraction properties vary under the influence of inflammation and reduction in the proximity of various analytes (Figure 14e,f). Moreover, it can be functionalized by methacrylic acid that reversibly captures H$^+$, to sense any changes in pH.

Hayashi et al.[92] have shown that the DNA aptamer–linked polyacrylamide (PAAm) hydrogel is able to sense biochemical materials and provide chromatic data repeatably. By exposing the structure to different concentrations of a silver acetate solution,

the DNA aptamer–linked PAAm hydrogel presented shrinkage based on the concentration. As a consequence of the changes in the spatial distance between the nanostructures during shrinking or swelling of the hydrogel, the reflected color is shifted.

Deng et al.[93] demonstrated the use of structural color as a real-time monitor of in situ drug release. They developed a molecular-imprinted therapeutic contact lens with structural color, comprising SiO$_2$ monodisperse particles arranged in an organized manner. This device could enable monitoring of drug release by color change (Figure 15a). The porous structure generates a diffractive color that upon drug release and contraction of the structure undergoes a blueshift in the Bragg diffraction peak. As such, the degree of the drug (i.e., timolol) release can be monitored by the visible color alteration of the lens.

The visualization of mechanical sensing can extend the application to position detection and tracking of a movable object.
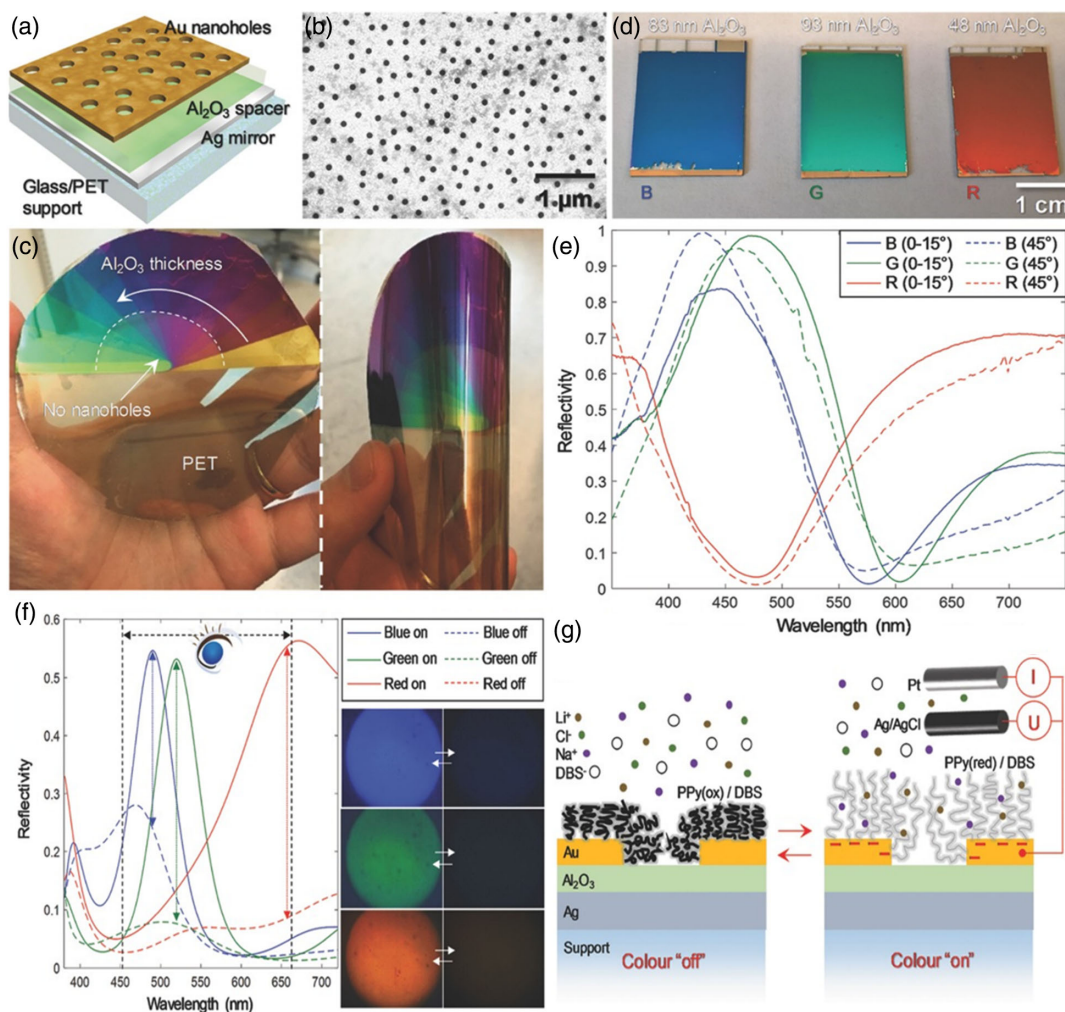
**ADVANCED
SCIENCE NEWS**

www.advancedsciencenews.com

**ADVANCED
PHOTONICS
RESEARCH**
Open Access

www.adpr-journal.com

Figure 13. Reflective color electronic papers. a) Schematic illustration of the plasmonic metasurface structure; b) The electron microscopy image shows the arrangement of the nanoholes. c) A camera image of the plasmonic metasurface on a PET support with a color palette induced by altering the alumina thickness. d) A camera image of samples with the RGB colors under ambient light. e) Measured reflection spectra of the RGB samples illuminated at different incidence angles. f) Left: reflectivity of the RGB samples (0°–14° viewing angle) in the bright and dark modes. Note, the dashed lines imply the wavelength range wherein the luminosity function for photopic vision exceeds 5% of its maximum. Right: microscope camera images of the RGB samples in the bright and dark modes under equal illumination and brightness/contrast conditions. g) Reflection modulation by the formation of a polypyrrole film on the gold nanohole array. Note, the polypyrrole film's optical absorption can be adjusted by applying a voltage. Reproduced with permission.[85] Copyright 2016, John Wiley and Sons.

Park et al.[94] have demonstrated a strain sensor that visualizes mechanical loading based on a strain-sensitive structural color. To make the sensor's response visible, a mechanochromic bilayer of ionic gel (IG) is inserted in polydimethylsiloxane. The designed sensor is red in its relaxed form but turns blue when it is stretched to its maximum, resulting in a full-color alteration as a function of the strain (**Figure 15**b). The authors showed that the sensor was applicable as a reflectively visible electronic skin, visualizing the motion of a finger, elbow, and knee.

4. Polarizonic Reflective Coloration

In contrast to the localized plasmon that is characterized by absorption and scattering of an oscillated dipole, which is

an intrinsic property and does not consider the cooperative action of all matter (e.g., near-field response, hotspot generation), polarizonics is an exceptional field that emerges from the cooperative and coherent interactions and interference of oscillating bounded dipoles of polarized materials. Elbahri's group has verified this hypothesis[31,36,37,39,40] both theoretically and experimentally and shown that a sheet of oscillated dipoles, "nanoparticles, atoms, or molecules," behaves as a deterministic chaotic system that creates a macroscopic coherent response by the cooperative interference of the eigenvibrations. Thus, these random dipoles act as "artificial galaxies" with specular reflection in the Z direction, as observed on smooth conductor surfaces, but not yet reported for disordered ultrafine particles.
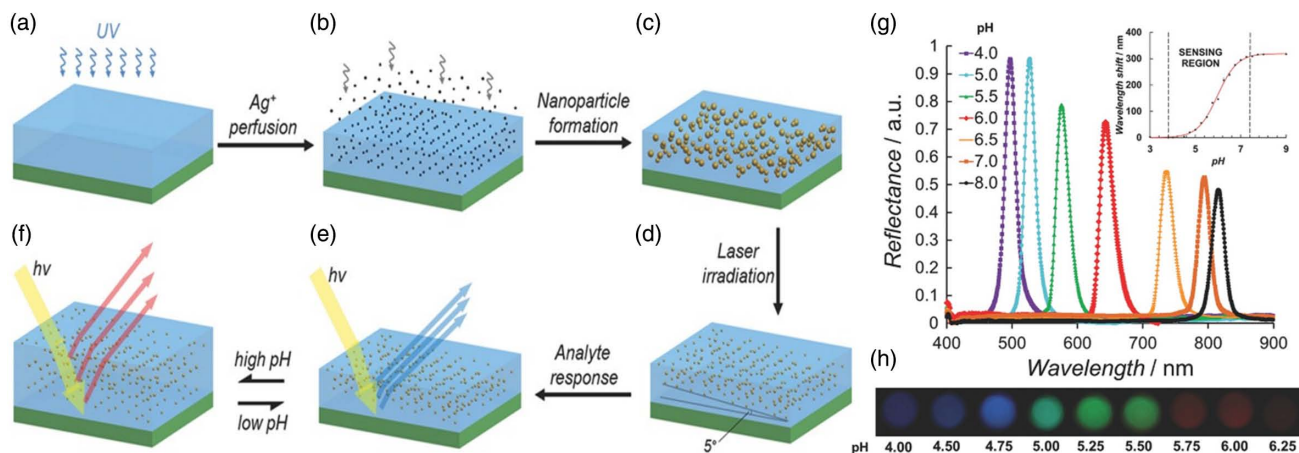
Figure 14. pH sensing by a diffractive holographic sensor. The multistage fabrication process of the holographic sensor. a) Polymerization of HEMA monomers functionalized with carboxyl groups on an O_2 plasma–treated PMMA substrate. b) Perfusion of Ag^+ ions into pHEMA film. c) Reduction of Ag^+ ions to Ag^0 nanoparticles within the pHEMA film by a photographic developer. d) Photochemical patterning of pHEMA–Ag nanoparticle composite using a single 6 ns Nd:YAG pulsed laser beam, elevated at 5° from the normal and backed by a mirror. e) pH-induced swelling/shrinking of the sensor changes the interparticle spacing and the refractive-index contrast, and thus displaces the diffraction peak from 500 to f) 815 nm upon expansion of the hydrogel. g) Measured diffraction spectra of the sensor swollen at different pH values. The maximum wavelength shift takes place at 815 nm and the minimum at 495 nm. The inset graph implies the sensor's response after three trials. h) Camera images of the pH holographic sensor exposed to phosphate buffers of pH 4.00–6.25. Reproduced with permission.[91] Copyright 2014, John Wiley and Sons.

4.1. Background

In the beginning, we should shed light on the meaning and conditions of occurrence of polarizonic resonance. Polarizonics originates from dynamic electronic polarization whereas *polarizonic resonance* is a phenomenon that occurs when a *bounded system* is driven to *oscillate at a specific frequency*, which leads to the *radiation of electromagnetic waves into the far field*. In this regard, the applied electric field from the inbound electromagnetic (EM) radiation will drive the electron cloud off from its positive core, whereas the charge attraction would create an opposing restoring force. The interplay between the applied force and the restoring force establishes the oscillations that can be regarded via employing the classical spring model as determined by Lorentz (Figure16a). The oscillation of the dipole will generate a changing electric field, which induces a fluctuating magnetic field propagating outward as an electromagnetic wave from the surface of the dipole. This picture is valid for any oscillated dipole, including metals[38] and dielectrics.[37,39]

When an atom, molecule, cluster, or small nanoparticle whose size is much smaller than the wavelength ($\lambda/d < 0.1$) is exposed to EM radiation, the field distribution across the entire object is considered homogenous according to the quasistatic approximation proposed by Lord Rayleigh.[95] In contrast, when a set of dipoles with close spacing is exposed to an external field at their resonance frequency, an enhancement of the response of a system occurs and the electronic clouds behave cooperatively. As a result, the induced waves from the individual excited dipoles would interfere and their near-field radiation pattern overlaps, resulting in a coherent cooperative action. **Figure 16**c,d shows the near-field radiation of a single dipole (c) in comparison to the coupled multiple dipoles (d) within near proximity. This coupling results in the spatially and temporally coherent radiation

modes that differ completely from the radiation mode of its single constituents. In other words, the ensemble of dipoles that are within near proximity of each other acts cooperatively at the microscopic level to produce a specular reflection at the macroscopic level. Similarly, a sheet of charges or so-called dipolar composite[31,37] would yield in the locally changing electric and magnetic fields inducing electric dipolar and quadrupolar moments which end up with a specular reflection in the far field.[96,97]

Commonly, the dipole oscillation has been studied with respect to the static electronic polarizability as a method of simplification. However, only via the dynamic electronic polarization (Figure16), a glimpse of the whole picture is achieved.

The dynamic polarizability based on the spectroscopic conformity principle can be described as[98]

$$\alpha(\omega) = \frac{e^2}{m} \sum_n \frac{f_{n0}}{\omega_{n0}^2 - \omega^2 - i\omega\delta_{n0}} \tag{3}$$

where δ_{n0} is the damping constant, ω_{n0} is the eigenfrequency, and f_{n0} is the oscillator strength. Under the condition of resonance where the external field frequency matches one of the eigenvibrations of the transition oscillator, i.e.,$|\omega - \omega_{n0}| \le \delta_{n0}$, the expression can be rewritten as follows

$$\alpha_{\text{res}}(\omega) = \left(\frac{e^2}{2m\omega_{n0}}\right) \frac{f_{n0}}{\omega_{n0} - \omega - \delta_{n0}/2} \tag{4}$$

Thus, the resultant of the resonant polarizability is a complex value whose real part represents refraction and reflection and is dependent on the illuminated material, being positive for dielectrics and negative for metals, whereas the imaginary part represents the absorption of the incoming radiation and is proportional to the restoring force of the oscillator (i.e., damping
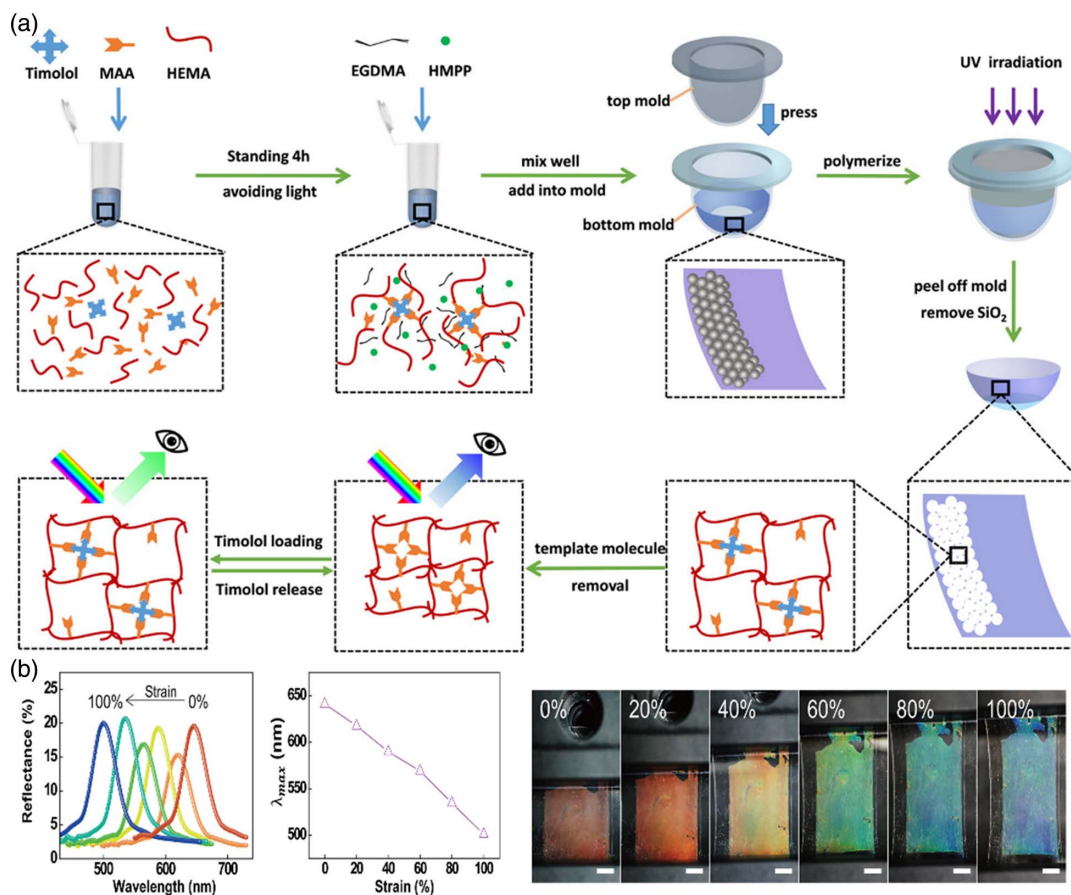
**ADVANCED
SCIENCE NEWS**

www.advancedsciencenews.com

**ADVANCED
PHOTONICS
RESEARCH**
Open Access

www.adpr-journal.com

Figure 15. Dynamic reflective color–based sensors. a) Schematic of the fabrication procedure of a molecular-imprinted structural color contact lens along with its working principle.[93] Reproduced with permission.[93] Copyright 2018, American Chemical Society. b) Reflectance spectra of a strain-based structural color sensor as a function of strain along with camera images of the sensor under different mechanical loads (all scale bars represent 1 cm). Reproduced under the terms of the CC BY license.[94] Copyright 2018, The Authors, published by Springer Nature.

constants). Therefore, both specular reflection and absorption occur simultaneously at resonance, which is associated with the free (metallic nanoparticle) and bound electrons of the resonating dipole. Consequently, the arrangement of the dipoles within a matrix does not affect or vary the specular reflection, yet the main contribution emerges from the dynamic polarizability of the arbitrary nanoparticles within the glassy medium as demonstrated by us[37,38,98] and adapted by other researchers.[99,100]

The complex refractive index (RI) of the effective medium of the nanocomposite plays a crucial role in the optical behavior of the stacked system. In this regard, the imaginary part "k" is governed by absorption, thus engendering the well-known plasmonic colors. In contrast, during a real part "n" domination that expresses reflection, the polarizonic specular reflection emerges conveying vivid colors to the far field as shown in **Figure 17**.

4.2. Polarizonics in Metal Nanoclusters and Nanocomposites

Recently, we[31] have succeeded to create amorphous metasurfaces for structural reflective coloration based on randomly distributed Ag nanoparticles on a blackbody (**Figure 18**a). In such a

structure, the tiny plasmonic dipoles as small as <10 nm are already famous for their strong absorption potential.[7] In this regard, the polarizonic specular reflection occurring at the resonance frequency can be utilized to create radiant plasmonic colors, without the need to employ complicated production and lithography methods.[57,69,101] The interference of the radiating Hertzian dipoles[102,103] occurring at the microscopic level and induced by fluctuations of charges[37] outcomes as a spectacular specular reflection. The synergistic oscillation of the dipoles results in cooperative dipolar coupling, thereby a resonating specular reflection, despite the random arrangement of the dipoles or their residence on a blackbody. The presence of several dipoles in near proximity and the intersection of their radiation patterns give rise to a dipolar photonic event.[37,104] Concerning the specular reflection effect, the Ag-based plasmonic nanocomposite can potentially generate a blue color, which is hardly perceived by the naked eye. For the sake of visualization, we used a black substrate that could hamper both transmission and diffuse scattering, thus the color develops solely from the specular polarizonic reflection (Figure 18b). In fact, the surrounding sensitivity of the polarizonic reflection color is much higher compared to that of the transmitted/extinct response as a result of the
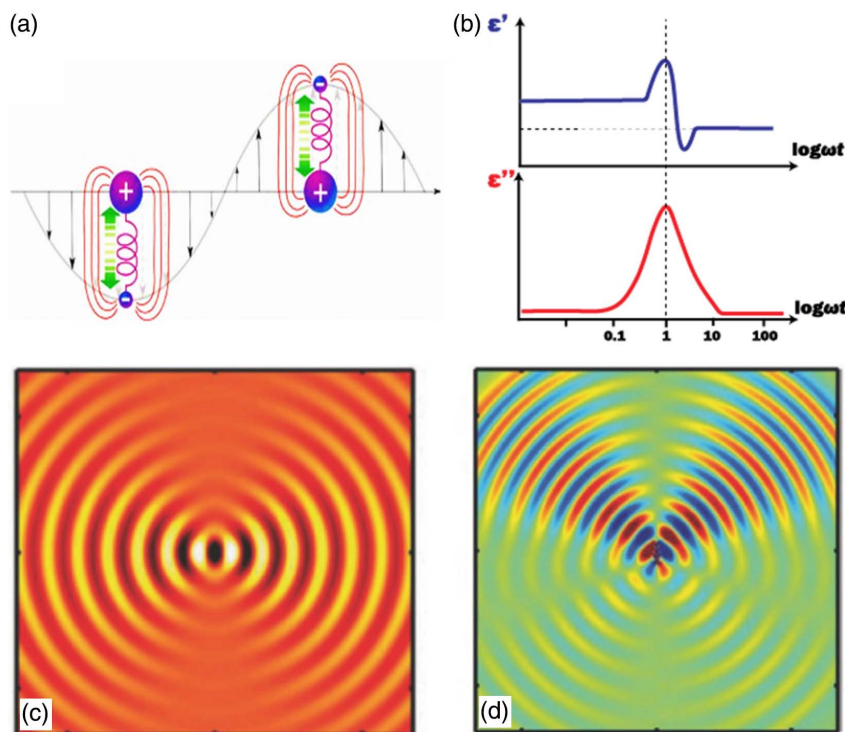
**ADVANCED
SCIENCE NEWS**

www.advancedsciencenews.com

**ADVANCED
PHOTONICS
RESEARCH**
Open Access

www.adpr-journal.com

Figure 16. a) An illustration of a driven Lorentzian oscillator exposed to an external electric field. Reproduced with permission.[37] Copyright 2015, The Authors, published by Springer Nature. b) Dynamic electronic polarizability. c) A schematic of a Hertzian dipole radiating electric field; d) six Hertzian dipoles in close proximity demonstrating interference and directional light propagation. Reproduced with permission.[31] Copyright 2017, John Wiley and Sons.
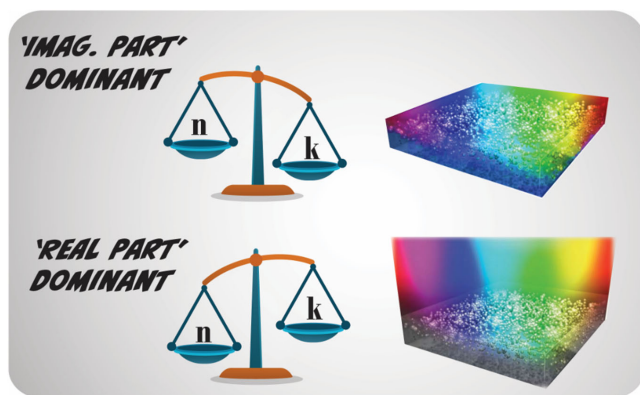

Figure 17. The interplay of the real and imaginary components of an optical system in identifying its properties, wherein an imaginary dominant arrangement of plasmonic colors is presented. However, in a "real part" dominant system, a vivid polarizonic specular reflection appears.

propagation delay. As shown in Figure 18c, the naked-eye perception of color and the contrast of the $(SiO_2)_x/(AlN)_{1-x}$-coated Ag nanoparticles in transmission mode is not easy. However, distinct vivid colors are readily visible on a blackbody as observed in Figure 18d, thus emphasizing a promising environmental sensitivity.

The polarizonic sensing is unique with regard to the far-field radiation of the dipole antenna that is capable to store and

transfer information at a certain color that merely depends on the propagation delay. Moreover, by altering the real part of the refractive index atop the antenna, thus the speed of the wave's propagation, different polarizonic radiation colors appear, while the nanoparticle's plasmonic color does not change remarkably. Therefore, the polarizonic concept enables the detection of the conformational change of a surrounding environment even in the bulk state (**Figure 19**).

Inexpensive biosensors that enable rapid (real-time) recognition of bioanalytes are highly demanded for many applications such as instant disease diagnosis, point-of-care (POC) clinical evaluation, and genetic analysis for precision medicine. This demand has directed the progress of an innovative class of biosensors for personal monitoring and POC applications. Such sensors have been developed based on advanced microelectromechanical system (MEMS) technology allowing fluid guidance in microscaled channels, computerized chemical and biochemical processes, as well as optofluidic integration.[105,106] For the lattermost option, the plasmonic biosensors have shown promising applicability for the detection of a diverse range of biological molecules with single-molecule sensitivity based on RI monitoring.[107] The biosensors performing based on surface plasmon resonances (SPRs) are extremely sensitive to the dielectric materials in the proximity of the metallic surface. However, sophisticated plasmonic biosensing methods have not been efficient in the detection of volume binding of analytes based on bulk RI monitoring.[108] Therefore, bulk detection, which is important
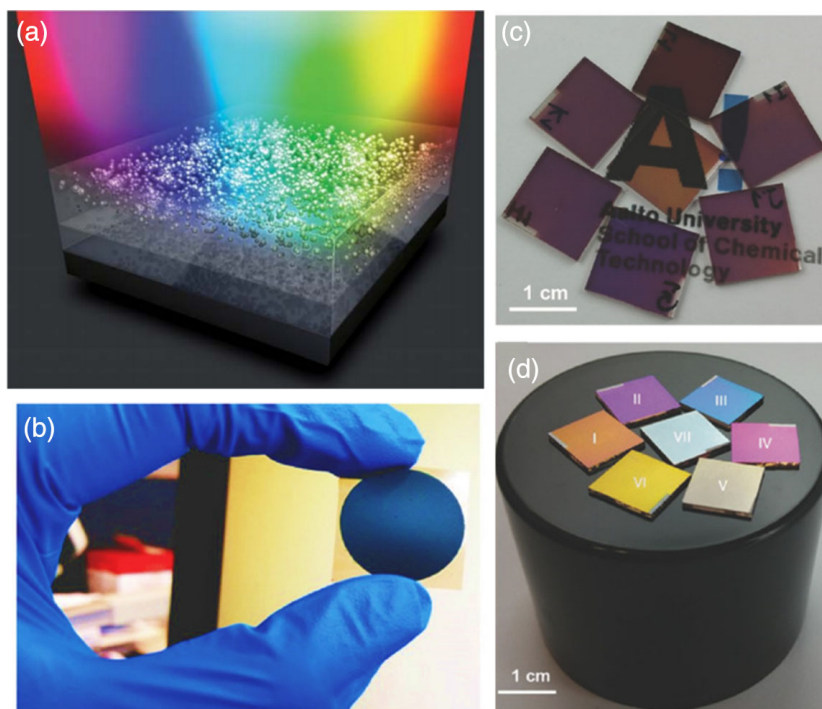
Figure 18. Specular reflection–based color for environmental detection. a) Schematic illustration of specular reflective and plasmonic colors generated by the dipoles. Reproduced with permission.[117] Copyright 2014, The Royal Society of Chemistry. b) A true image of a silver nanocomposite deposited on a carbon tape. c,d) The camera images of the samples comprising the nanoparticles coated with a composite layer of SiO_2 and AlN, illuminated in transmission and reflection mode, respectively. The labeled samples' thickness and compositions are as follows—I: 60 nm (70% AlN/SiO_2); II: 80 nm (50% AlN/SiO_2); III: 80 nm (70% AlN/SiO_2); IV: 80 nm (AlN); V: 80 nm (SiO_2); VI: 60 nm (50% AlN/SiO_2); and VII: no dielectric coating. Reproduced with permission.[31] Copyright 2018, John Wiley and Sons.
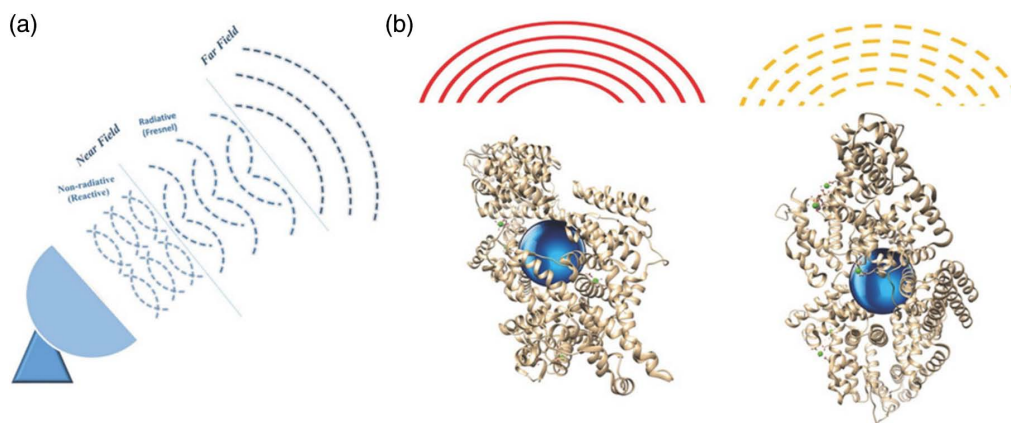

Figure 19. The optical sensing mechanism of the plasmonic dipoles. a) Schematic illustration of the dipoles as nanoantennas. b) The schematic shows how conformational change of the bovine serum albumin protein alters the speed of the wave propagation, and thus the emerged polarizonic color. In contrast, the plasmonic color of the dipole is not affected. Reproduced with permission.[31] Copyright 2018, John Wiley and Sons.

for POC tests and immediate, inexpensive clinical evaluations, has not been realized in practice. The main cause for this bottleneck is that the plasmonic coupling governs local near-field enhancement that decays exponentially in a few nanometers.[109–112] Accordingly, the presence of any adjacent molecule whose size is not over the decay span can be optimally sensed. In contrast, the change induced by such a substance in the near field cannot be recognized by a far-field observer. This means that any microscopical variation in the medium surrounding the plasmonic material is not detectable in a bulk state.[113]

In a recent study,[31] we realized the first naked-eye recognition of biological analytes based on the relative changes in the bulk refractive index. The bulk detection takes place based on the RIs' real-part variations at the polarizing angle instead of the imaginary part changes utilized by the conventional LSPR

ADVANCED
SCIENCE NEWS
www.advancedsciencenews.com

ADVANCED
PHOTONICS
RESEARCH
Open Access
www.adpr-journal.com

methodologies. The detection of the biological environment is based on the coupling between the stimulated dipoles (here, Au nanoparticles) and the induced dipole of the enclosing matrix,[11] where the polarizability and concentration of the molecules are easily identified by the plasmonic Brewster wavelength (PBW). In the case of irradiation of polarized white light at an incidence angle below the "plasmonic" Brewster angle, a naked-eye detection of the biological analytes is realized, beyond which the penetration of p-polarized light into the sample allows for volumetric-based detection.

As a proof of concept, our approach could enable naked-eye sensing of healthy and diseased exosomes in reflection modes at the Brewster angle (**Figure 20**a). Such an achievement is not realized in the extinction/transmission mode (Figure 20b, c), or by the available transduction plasmonic detection methods of exosomes.[24,101,114] To validate the feasibility of the PBW method for clinical biodetection, the shift of p-polarized light's wavelength ($\Delta\lambda$) when exposed to the healthy and diseased (inflammatory bowel disease) exosomes were quantified. Figure 20d,e implies that $\Delta\lambda$ in the transmission mode is slight (<20 nm), whereas it approaches $\approx$232 nm at the Brewster angle stressing the high sensitivity and the dependency of the PBW on the medium's polarizability. Figure 20f shows the analytical sensing performance of the PBW sensor in both the transmission and Brewster modes. As clearly deduced from the slopes of the linearly fitted lines, sensitivity of the biosensor in the Brewster mode is remarkably larger. The biosensor's limit of detection (LOD) was measured via LOD $= 3S/M$, where S is the standard deviation and M is the slope of the linear fitted curve.[115] The ratio of

the slopes of the linear sensing performance in the Brewster and transmission modes indicated the Brewster sensitivity enhancement factor (EF). The Brewster sensitivity EF of 412.3 and the much smaller LOD of 4.16 stress the extraordinary bulk biosensitivity in the Brewster mode compared to that in the conventional transmission mode (LOD of 214.28). As deduced from the obtained LOD measurements, our PBW technique is not as sensitive as the LSPR or SPP methods; however, it can be regarded as a real-time, easy, and quick sensing method for diagnosing dangerous diseases with simple visible feedback.

4.3. Polarizonic Interference: Form Substrate-Insensitive Optical Response to Colored Solar Perfect Absorber

The optical properties of metals are typically described by a continuous field through the Drude model, which relates the reflectivity to be solely dependent on the number of free electrons (i.e., conductivity). Despite its popularity and applicability to most gray metals, this theory is unable to explain the unique colors of gold or copper. In contrast, the classical Drude–Lorentz theory assigns a discontinuous state to the sea of electrons considered by the Drude model given that the bounded electrons are regarded as driven Lorentzian oscillators, which radiate a polarizonic color to the far field when exposed to an EM wave at a specific frequency.[31] Accordingly, the metal's optical property is governed by the gray color arising from the broad reflection of the "continuous state" along with the localized polarizonic reflection of the "discontinuous" state.[116] Consequently, the presence of both states ensues a quantum interference that causes a drop in the
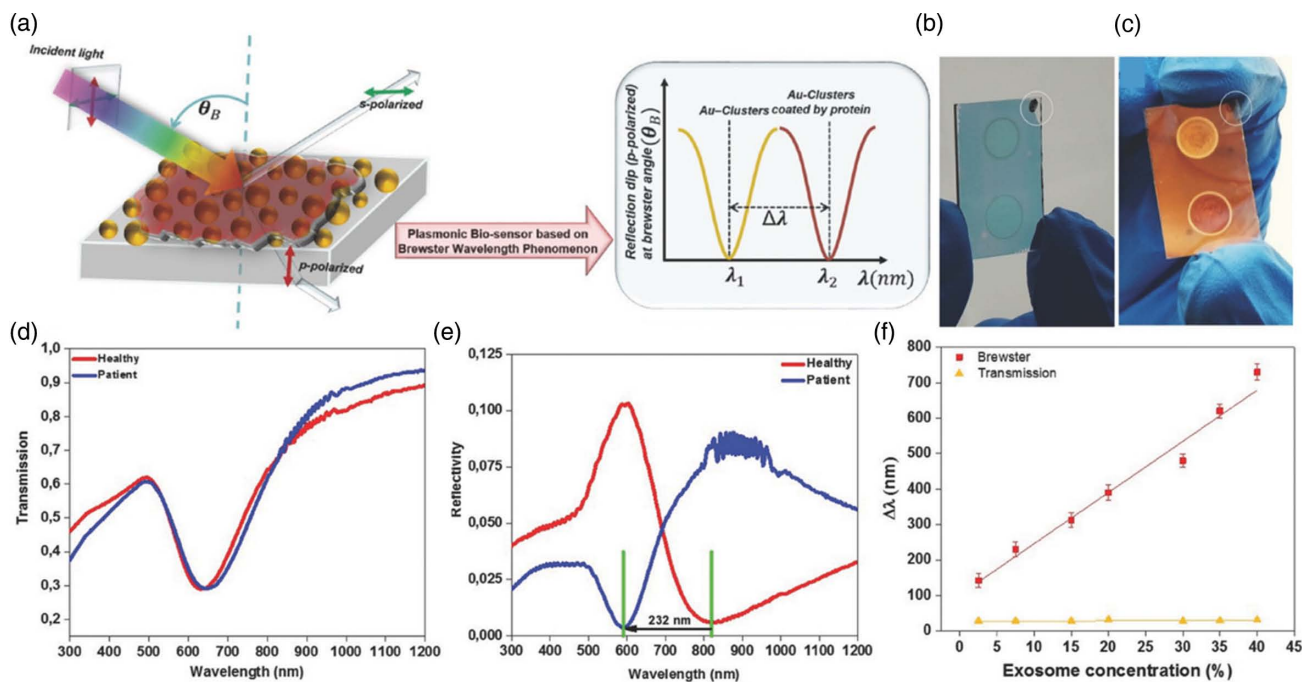

Figure 20. Naked-eye detection of diseases by a specular reflection–based biosensor. a) An illustration showing the sensing mechanism in the Brewster mode. b) Transmission and c) reflection images of the nanocluster exposed to healthy (bottom) and diseased (inflammatory bowel disease, top) serum exosomes. d) Transmission and e) reflection (at 70°) spectra of the biosensor exposed to healthy (red line) and diseased (blue line) serum exosomes. f) The linear correlation between the wavelength shifts ($\Delta\lambda$) and exosome's concentration in transmission and plasmonic Brewster modes. Note, in transmission mode the error bars ($n = 3$) are as high as the symbols. Reproduced with permission.[31] Copyright 2018, John Wiley and Sons.

**ADVANCED
SCIENCE NEWS**

www.advancedsciencenews.com

**ADVANCED
PHOTONICS
RESEARCH**

www.adpr-journal.com

reflection at the plasma frequency, thus explaining the color of gold. However, the nonappearance of the polarizonic reflection at the visible spectrum dictates the gray color of many metals including silver and aluminum.

Based on the aforementioned concept, whenever plasmonic nanoparticles exhibiting a localized polarizonic reflection "discontinuous state" interact with a broad reflection of a gray metal or a semimetal "continuous state," a polarizonic interference occurs that is independent of the type of the gray metal (**Figure 21**a).

To fully utilize and experimentally prove the polarizonic interference, we mimicked the optical and visual properties of gold, by deploying Ag nanocomposite on a metal substrate as shown in Figure 21c. When the Ag–SiO$_2$ nanocomposite is deposited on glass, it produces a polarizonic reflection around the blue part of the visible spectrum, as shown in Figure 21b, which is the same frequency range at which gold experiences its quantum

interference between the continuous reflection arising from its free electrons and the localized reflection emerging from its oscillating dipoles at the plasma frequency. Thus, by allocating this Ag–SiO$_2$ nanocomposite on a board reflector such as aluminum, silicon, or stainless steel, a golden omnidirectional, polarization- and substrate-independent specular coloration was obtainable. Figure 21d,e shows the finite difference time domain (FDTD) simulations, where it is clear that the observed color is due to the polarizonic and the dipolar destructive interference.

For instance, the FDTD simulation of the 20 nm Ag nanocomposite[104] can validate the outstanding properties of these dipoles and their communication with the silicon substrate. Figure 21d shows the electromagnetic confinement and guiding occurring among an ensemble of 5 nm silver nanoparticles that are embedded in a 20 nm thick dielectric matrix. However, once the nanocomposite is overlaid atop a semiconducting surface of, e.g., silicon, as shown in Figure 21e, the electromagnetic fields are
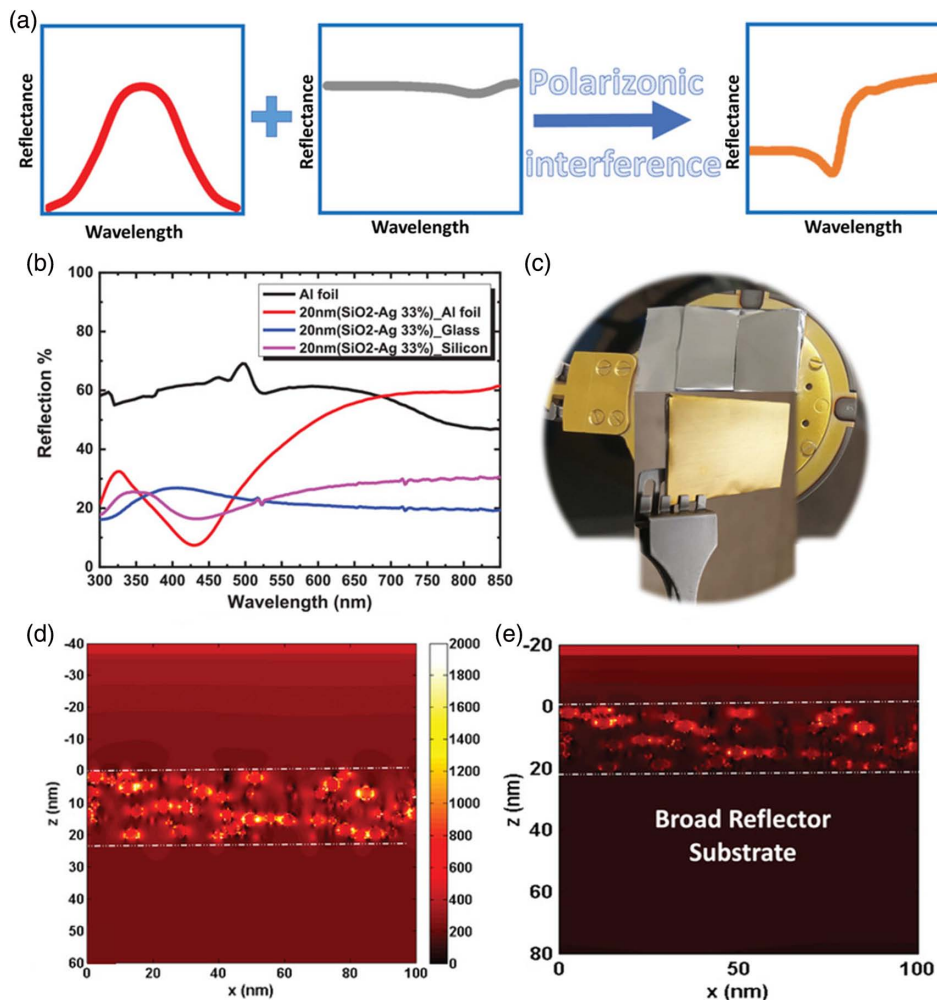

Figure 21. The polarizonic interference phenomena. a) An illustration showing the polarizonic phenomena as a result of the interference between the continuous reflection and the localized reflection. b) Reflection spectra of the silver nanocomposite on multiple surfaces along with the spectra of an aluminum foil. c) Photograph showing the golden color of the nanocomposite on the Al foil and the substrate holder of the magnetron sputtering system along with the color of the bare aluminum foil. d,e) The FDTD simulation at 430 nm of a 20% Ag/SiO2 nanocomposite (monodispersed particles of 5 nm) showing the electrical field distribution, where (d) is on standalone mode and (e) as deposited onto a silicon substrate. Reproduced with permission.[38] Copyright 2019, John Wiley and Sons.

diminished, confirming the dipolar destructive interference and the polarizonic interferometry response. The dipolar interference occurs due to the dipole–image interaction and governs the design of an omnidirectional polarizonic interference.

It is worth mentioning that by shifting the polarizonic resonance (i.e., changing the filling factor of the Ag nanocomposite), the color of the bilayer can be tuned. For instance, the golden appearance of the 33% Ag was shifted to a titan silver at 20% Ag on the aluminum kitchen foil.

Similarly, polarizonic interference can be used for a new generation of colored solar absorbers. By tuning the type and filling factor of the plasmonic structures as well as their host composition, a wide range of vivid colors with almost perfect absorption is attainable, as shown in **Figure 22**. In fact, the perfect absorption and the color arise solely from the nanocomposite overlay. By increasing the filling factor of the nanocomposite, the reflection dip redshifts as a result of the increasing size of the particles and their interactions. Although altering the environment type affects the coupling between the dipoles and the polarizable medium and results in a new appearance of the absorber that has changed from shiny by TiO_2 to matt by SiO_2. Additionally, the color of the bilayer structure can be tuned by varying the nanocomposite thickness or via annealing as reported by Byun et al.,[99] who succeeded in generating four vivid colors (magenta, blue, yellow-green, and orange) arising from the polarizonic interference of the amorphous gold–alumina nanocomposite with a gray stainless-steel substrate.

4.4. The Polarizonic Broad Antireflection Coatings (ARCs) and the Interplay between n and k

ARCs are crucial for many optical and optoelectrical applications. Despite their attractive merits, they show many shortcomings with respect to the impedance of the beneath layer and the need for a precise thickness. In this regard, one promising potential solution could be the development of a broad polarizonic ARC.

To devise such a coating, the dynamic polarizability of the resonating Lorentzian oscillators, where the real part exhibits normal and anomalous dispersion, is coupled with optical behavior of a nonabsorbing dielectric whose refractive index lies between the normal and the anomalous dispersions (i.e., $n_{\text{dispersive}} < n_{\text{dielectric}} > n_{\text{anamalous}}$) and approximately is equal to $n_{\text{PAC}} = \frac{n_{\text{dispersive}} + n_{\text{anomalous}}}{2}$.

Based on the bilayer configuration of resonating dipoles on top of a dielectric film, an antireflection property arises. In such a structure, when the frequency of the incident radiation is less than the resonance frequency of the dipoles, the system behaves as a gradient-index antireflection coating ($n_{\text{top}} < n_{\text{spacer}}$), whereas at frequencies above their resonance ($n_{\text{top}} > n_{\text{spacer}}$), the coating is transformed to a F–P interferometer in which the thickness of the sublayer plays a crucial role in the development of a totally destructive interference (**Figure 23**a). This postulate is valid for any kind of material. Figure 23b shows the reflection contour calculated via the FDTD method at 600, 800, and 900 nm, respectively, for a 20 nm layer of an arbitrary material deposited on top of a SiO_2 layer, all on a silicon substrate. Regardless of the high RI ($\approx$3) of the coating and the thin SiO_2 sublayer, a suppressed reflection is apparent at thicknesses far below the quarter of the design wavelength of 600 nm. In addition, an increase of the sublayer thickness while keeping the RI approximately the same results in a redshift of the suppressed reflection.

Relying on the aforementioned concept, we[117] demonstrated the first polarizonic antireflection bilayer coating based on an Ag–SiO_2 nanocomposite atop a SiO_2 sublayer as shown in the TEM images (**Figure 24**a,b). The RI of the nanocomposite composed of ultrafine metallic nanoparticles ($d < 5$ nm), exhibiting normal and anomalous dispersion (Figure 24c), is controllable based on the filling factor, thickness, and type of its constituents, therefore enlightening a novel method to engineer ARCs. Consequently, the visible reflection originating from the silicon substrate was diminished by an ultrathin (20 nm) stack of Ag nanocomposite ($n_{\text{dispersive}} = 2.1$, $n_{\text{anamalous}} = 1.2$) on top of a 50 nm SiO_2 sublayer ($n_{\text{PAC}} \approx n_{SiO2}$), as shown in the red curve of the reflection spectra in Figure 24d, whereas the blue curve
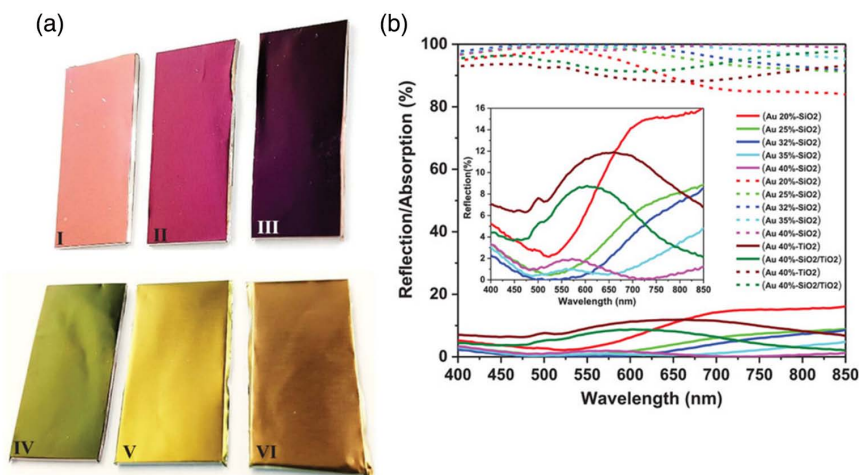

Figure 22. Colored perfect solar absorbers based on the polarizonic interference phenomenon. a) Camera images of vivid colors of a gold nanocomposite with different filling factors and hosts. The composition of the gold nanocomposites were as follows—I: 20% (Au/SiO2); II: 25% (Au/SiO2); III: 32% (Au/SiO2); IV: 40% (Au/SiO2); V: 40% (Au/TiO2); and VI: 40% Au/(TiO2/SiO2). b) Reflection/absorption spectra of the colored absorbers. Reproduced with permission.[38] Copyright 2019, John Wiley and Sons.

**ADVANCED
SCIENCE NEWS**

www.advancedsciencenews.com

**ADVANCED
PHOTONICS
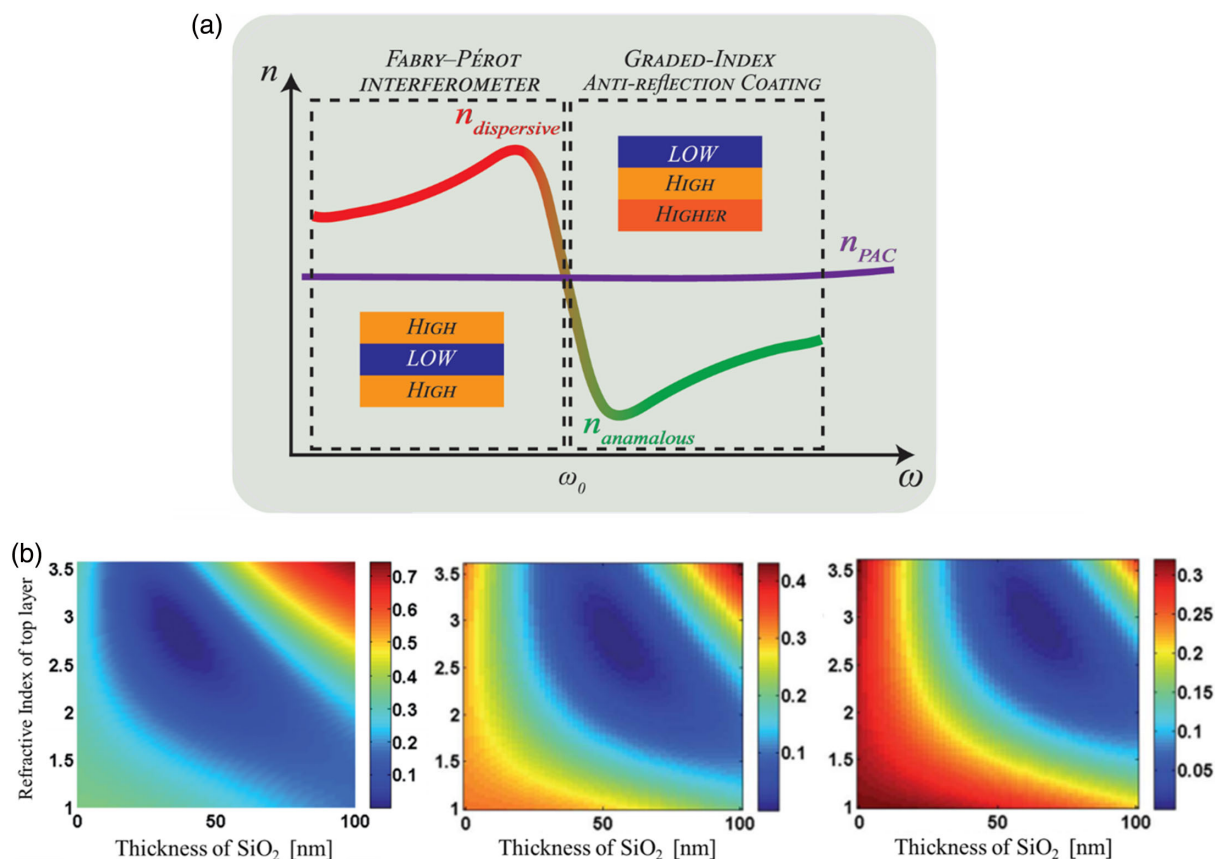RESEARCH**
Open Access

www.adpr-journal.com

Figure 23. The working principle of the polarizonic ARC. a) The schematic shows the dual functionality of a polarizonic ARC. b) Reflection contour of a 20 nm thick film with varying RI on top of a SiO_2 layer in several thicknesses, calculated via the FDTD method, at 600, 800, and 900 nm (right to left) wavelengths. Reproduced with permission.[117] Copyright 2014, The Royal Society of Chemistry.

represents a 30% Ag nanocomposite. The optimized bilayer structure whose apparent color turns black (inset) shows minimal angular dependency as per its angular reflectance measurements that are shown in Figure 24e. Moreover, the bistack reflectance demonstrates two dips in its spectra, the first occurring at a high frequency as a result of the graded-index ARC functionality ($n_{anamalous} < n_{PAC}$), whereas the second reflection dip occurs at a lower frequency emerging from the destructive interference of the reflected field ($n_{dispersive} > n_{PAC}$).

In addition, the bilayer configuration is readily tunable by exploiting the optical thickness ($OP = n \times d$), where n is the refractive index and d is the thickness of the layer. In this regard, by applying the nanocomposite above a metallic gold mirror and by keeping the spacer layer thickness constant, a rainbow of colors emerges depending on the filling factor of the nanocomposite, indicating the dominance of the real part of the complex RI. **Figure 25** (top) schematically illustrates the layered structure comprising a 20 nm Au–SiO_2 nanocomposite on top of a 25 nm SiO_2 layer overlying a gold mirror film and the colors generated corresponding to different reflection drops associated with several chosen filling factors. The shown vivid polarizonic colors emerge at 13%, 20%, 30%, 40%, 50%, and 60% filling factors corresponding to yellow, orange, brown, black, green, and light green, respectively.

Alternatively, the optical thickness is altered by manipulating the thickness of the spacer layer and keeping the filling factor of the top composite constant (i.e., a fixed refractive index) (Figure 25, bottom). Starting from the lack of a spacer layer, a polarizonic interference effect would arise, as discussed earlier, presenting vivid colors with nearly perfect absorption or mimicking the color of gold; however, the introduction and the increase in the thickness of the sublayer would induce destructive interference of the visible spectrum, leading to a perfect black solar absorber[118] or a broad ARC, whereas further increase would result in a redshift of the reflection peak, as confirmed by the FDTD simulations shown in Figure 23b.

4.5. Dynamic Polarizonic Response of Molecules and Brewster Wavelength for Matrices' Polarization Detection

Polarizonics is an extraordinary field that arises from the cooperative and coherent interactions and the interference of the oscillated bound dipoles that are found in artificial metal–like conjugated molecules. We demonstrate the polarizonic concept in a molecular system and therefore control spectral reflections at the visible region of the electromagnetic spectrum by utilizing stimuli-responsive molecular dipoles that undergo reversible change under dynamic light switching.[37] Photochromic
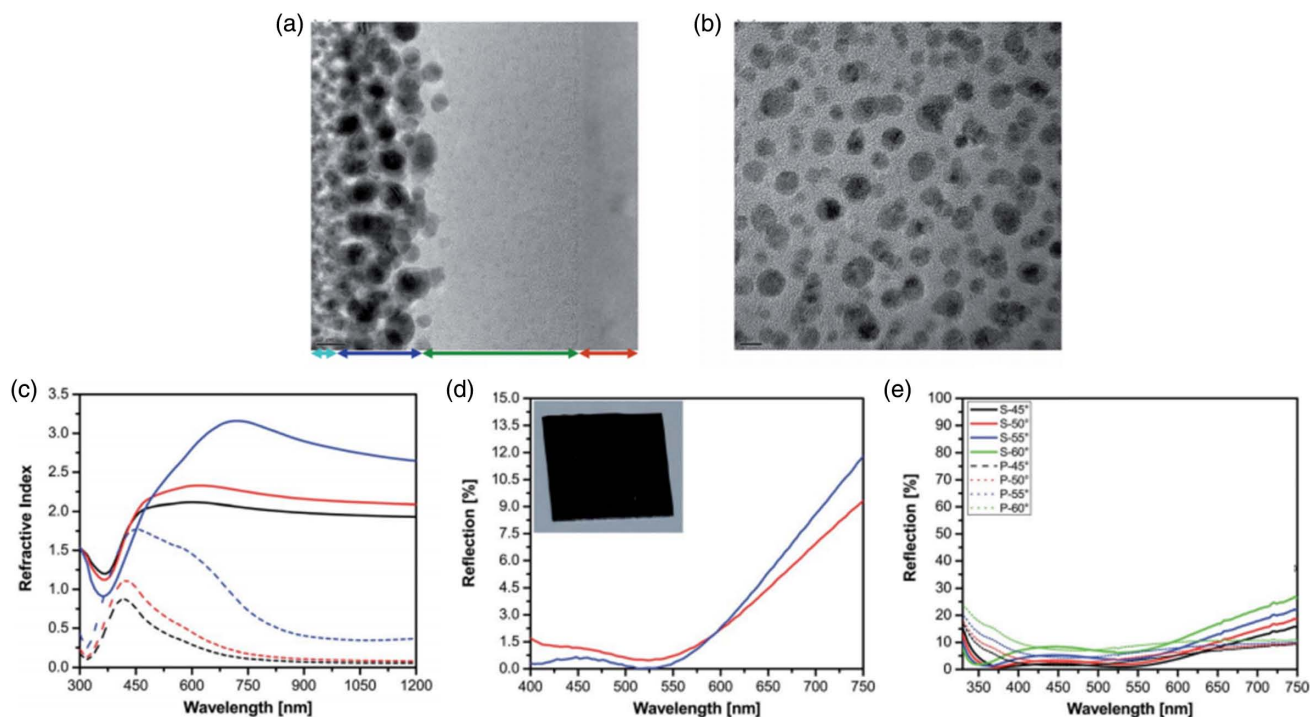
ADVANCED
SCIENCE NEWS
www.advancedsciencenews.com

ADVANCED
PHOTONICS
RESEARCH
Open Access
www.adpr-journal.com

Figure 24. Polarizonic ARC. a) Cross-sectional images of the plasmonic nanocomposites. The colored arrows indicate the thickness of each layer, representing light blue: Pt (top adhesive layer to cut the sample); blue: nanocomposite; green: SiO_2 layer; and red: silicon substrate. b) Top view of the fabricated sample and c) the complex refractive index of the nanocomposite at different filling factors. d,e) Reflection spectra of the deposited samples; the red and blue curves represent a 20% and 30% Ag nanocomposite, respectively. The inset is a camera image of the structure with a black appearance. Reproduced with permission.[117] Copyright 2014, The Royal Society of Chemistry.

molecules are active optical organic materials whose optical properties are controlled by external stimuli such as UV light. Indeed, most of the progress with the photoswitchable molecules, including spirophenanthroxazine (SPO), has been solely on the absorption arising from the electronic transition of these molecules. Regardless of its widespread spectrum of applications, some essential features and properties concerning these molecules are still to be explored. In 2015, we introduced the concepts of molecular dipole oscillation, cooperative coupling, and coherent radiation of organic molecules.[37] The collective electron displacements of the oscillating photoswitchable molecules are similar to plasmonic nanoparticles, yet they can be further intensified by UV irradiation that allows the conjugation of these molecules encompassing delocalized electrons (in the π–π* orbitals). As the frequency of light approaches the natural resonance of the molecule, a transfer of energy to the molecule permits its elevation into an excited state while simultaneously inducing an oscillating dipole of the polarizonic material resulting in a specular reflection at the visible region on the electromagnetic spectrum.

The dynamic switchability of the photochromic molecules ensures a dynamic polarizonic response where the reflection emerge or vanish upon illumination with UV or visible light, respectively. Furthermore, the polarizonics paved the way toward a novel criterion to engineer and detect the *molecular Brewster wavelength*, where a dip in the *p*-polarization reflection is detected as at a certain angle of incidence (**Figure 26**a).

When embedded in a different matrix, the switchable polarized reflection response of the molecules becomes a unique detection tool to detect the polarizability of the surrounding host, regardless of its impedance. In this regard, the surrounding matrices can be easily identified based on their dipole moments at a fixed angle (i.e., the Brewster angle), hence identifying a new term called the Brewster wavelength.[37] Figure 26b shows the reflection spectra at 45° and 65° for PS (polystyrene) and PVDF (polyvinylidene fluoride), both doped with SPO molecules. It is noteworthy that the reflection dip of the PVDF located at 640 nm is redshifted with respect to the PS at 65°. Although the RI of PVDF (1.42) is slightly less than PS (1.58–1.61), its dipole moment (2.1) is much stronger than the PS's (0.2–0.3), thus demonstrating a stronger coupling with the SPO molecules accompanied by a huge difference in its Brewster wavelength ($\Delta \approx 40$ nm). Based on this, the Brewster angle is identified by the ratio of mismatched refractive indices, whereas the Brewster wavelength is determined by the dipolar interaction between the embedded molecules and the surrounding matrix.

5. Limitation and Challenges

Despite the promising potential of reflective plasmonic coloration approaches, e.g., for full-color printing, they mostly suffer from a difficult fabrication process. EBL, as a standard fabrication method of plasmonic printing devices, is not only complex, slow, and costly, but also limited in the sample size. Thus, the
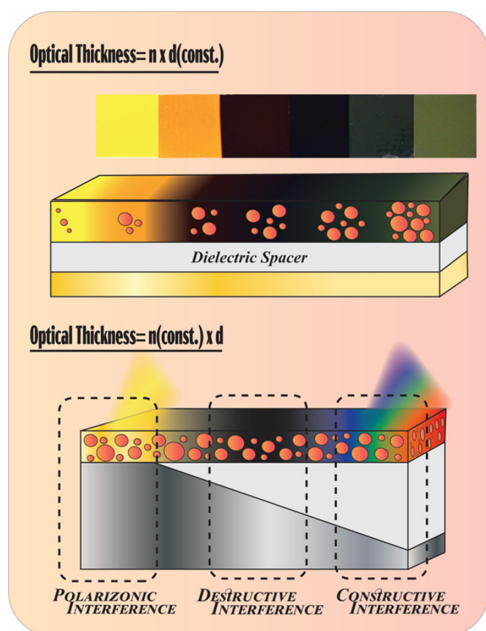
**ADVANCED
SCIENCE NEWS**

www.advancedsciencenews.com

**ADVANCED
PHOTONICS
RESEARCH** Open Access

www.adpr-journal.com

Figure 25. The effect of the optical thickness on the optical properties. (Top) An illustration showing the manipulation of optical thickness by varying the filling factor of the nanocomposite at a fixed spacer layer thickness, along with true images of a 20 nm Au–SiO$_2$ nanocomposite deposited on a 25 nm SiO$_2$ on top of a gold mirror. From left to right, the filling factors of nanocomposites are 13%, 20%,30%, 40%, 50%, and 60%, respectively. Reproduced with permission.[117] Copyright 2014, The Royal Society of Chemistry. (Bottom) The schematic shows the change in the optical thickness by fixing the refractive index and varying the thickness of the sublayer.

development of a productive method enabling full-color and scalable fabrication of reflective plasmonic color devices is highly demanded. This necessity is further stressed when dealing with the glassy polarizonic structures wherein the dispersion mode of ultrafine (<10 nm) plasmonic nanoparticles is a key factor. There is a need for fabrication methods that allow control over the arrangement of the nanoparticles as ordered and nonordered

and at different filling factors. Accordingly, they can tune the optical properties of the structure and coloration. In this regard, adjustment of the interference zone and spacing of the nanoparticles is an important requirement, particularly at high filling factors that could lead to higher reflectivity while avoiding severe aggregation. Induced by the inherent loss of metals in the visible spectrum, the reflection polarizonic peak is normally broad and weak. For the realistic, practical utilities, a high spatial resolution is as important as the brightness and color contrast.

The noble metals used for the generation of reflective colors should be durable and inexpensive. Also, they should comply well with the complementary metal–oxide semiconductor (CMOS) fabrication process and generate a full color. In this regard, gold is highly stable and resistant even at the nanoscale but unable to produce blue color due to its large transition band in the blue region of the visible spectrum. Copper is an unwanted plasmonic material for reflective structural coloration due to the coincidence of interband transition and plasmon resonance, leading to high damping of plasmon resonance.[119] Also, it undergoes oxidation whereby its optical properties (plasmon resonance) are altered.[120] Silver in contrast shows less Ohmic loss in the visible spectrum, yet is susceptible to oxidation[121] and sulfidation[122] in the ambient atmosphere that can degrade the generated color. Moreover, silver is not compatible with the CMOS fabrication process. Finally, aluminum can offer remarkable optical properties facilitating the generation of structural colors. However, it is oxidized promptly in air, and its oxide layer redshifts the resonance.[123,124] Thus, finding a suitable plasmonic material for reflective structural coloration is still a challenge and needs further research.

6. Conclusion

The reflection-based plasmonic and polarizonic colorations are still in their infancy as witnessed by the limited number of relevant articles in the literature. However, promising achievements in this area particularly for polarizonic vivid coloration by disordered dipoles will attract extensive attention of the scientific community in the near future. In this Review, the theoretical and practical points of view of the exotic polarizonic coloration
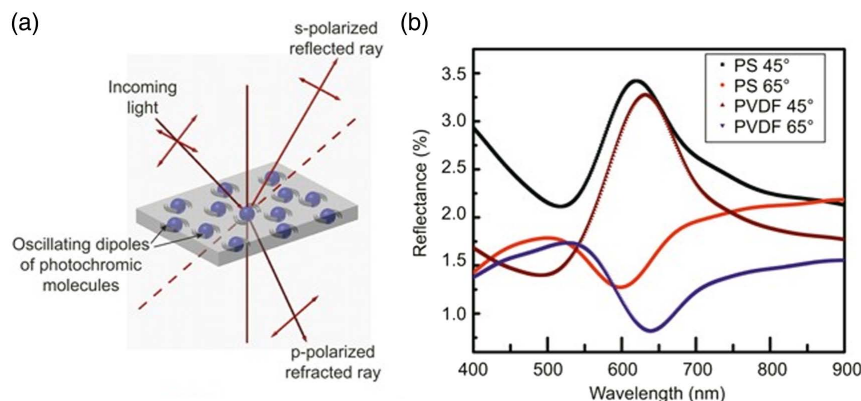

Figure 26. a) Schematics of the oscillating photochromic dipoles at the Brewster angle. b) Reflection spectra of an SPO-embedded PS (black, red) and PVDF (maroon, blue) nanocomposite at 45° and 65°, respectively. Reproduced with permission.[37] Copyright 2015, The Authors, published by Springer Nature.

**ADVANCED
SCIENCE NEWS**

www.advancedsciencenews.com

**ADVANCED
PHOTONICS
RESEARCH**
Open Access

www.adpr-journal.com

and interference along with its distinction from plasmonic were presented and highlighted. A myriad of new possibilities from disordered dipoles and ultrafine nanostructures are still to be explored as their properties can be altered by varying the size, type, and shape of the nanodipoles along with the material and type of the matrix (passive or active). Uniting these polarizonic nanomaterials with a facile, green, and scalable fabrication method such as magnetron sputtering realizes their huge potential in many fields such as solar energy harvesting, sensors, color filters, and flexible optical devices.

In this regard, future research will be oriented toward the production of brighter and high-contrast reflective colors that could be achieved by the replacement of metals with polarizonic dielectric nanostructures. Nature has made diverse bright and high-contrast structural colors based on dielectric nanostructures, as seen by the photonic crystals in peacock feathers,[125] butterfly wings,[126] opals,[127] and the pseudo-gap in birds' feathers.[128] In comparison to the plasmonic structural colors, and thanks to their superior reflectivity, the periodic dielectric nanostructures can produce much brighter and sharper structural colors.[129-131] Thus, it is expected to deal with a new class of reflective structural coloration systems based on lossless polarizonic dielectric pixels. Despite the mentioned merits of the dielectric nanostructures, the nature of polarizonic response in the disorder medium has been recognized with photoswitchable molecules, yet the negligible refractive index contrast still could be challenging. This obstacle can notably hamper the spatial resolution and thus the applicability of such structures in various utilities such as painting, textiles, and passive displays.[132,133] Accordingly, the resolution of this problem (i.e., generation of bright and high-contrast colors with practical spatial resolutions) should be diligently sought.

Conflict of Interest

The authors declare no conflict of interest.

[1] R. Hooke, *Micrographia: or Some Physiological Descriptions of Minute Bodies Made by Magnifying Glasses, with Observations and Inquiries Thereupon*, Courier Corporation, New York **2007**.

[2] H. Galinski, G. Favraud, H. Dong, J. S. T. Gongora, G. Favaro, M. Döbeli, R. Spolenak, A. Fratalocchi, F. Capasso, *Light Sci. Appl.* **2017**, *6*, e16233.

[3] J. A. Schuller, E. S. Barnard, W. Cai, Y. C. Jun, J. S. White, M. L Brongersma, *Nat. Mater.* **2010**, *9*, 368.

[4] H. A. Atwater, A. Polman. *Materials for Sustainable Energy: A Collection of Peer-Reviewed Research and Review Articles from Nature Publishing Group 3–11*, World Scientific Publishing Co., Singapore **2010**.

[5] S. Sun, Z. Zhou, Z. Duan, S. Xiao, Q. Song. in *2017 Conf. on Lasers and Electro-Optics, CLEO 2017 – Proc. vols 2017–January 1–2*, Institute of Electrical and Electronics Engineers Inc., Piscataway, NJ **2017**.

[6] A. Del Mazo Vivar, *Rev. Eureka* **2016**, *13*, 505.

[7] G. Mie, *Ann. Phys.* **1908**, *330*, 377.

[8] K. L. Kelly, E. Coronado, L. L. Zhao, G. C. Schatz, *J. Phys. Chem. B* **2003**, *107*, 668.

[9] P. K. Jain, X. Huang, I. H. El-Sayed, M. A. El-Sayed, *Plasmonics* **2007**, *2*, 107.

[10] L. M. Liz-Marzán, *Langmuir* **2006**, *22*, 32.

[11] S. Eustis, M. A. El-Sayed, *Chem. Soc. Rev.* **2006**, *35*, 209.

[12] W. L. Barnes, A. Dereux, T. W. Ebbesen, *Nature* **2003**, *424*, 824.

[13] A. V. Zayats, I. I. Smolyaninov, A. A. Maradudin, *Phys. Rep.* **2005**, *408*, 131.

[14] E. Ozbay, *Science* **2006**, *311*, 189.

[15] S. Kawata, Y. Inouye, P. Verma, *Nat. Photonics* **2009**, *3*, 388.

[16] J. A. Carter, D. C. Fabrycky, D. Ragozzine, M. J. Holman, S. N. Quinn, D. W. Latham, L. A. Buchhave, J. Van Cleve, W. D. Cochran, M. T. Cote, M. Endl, E. B. Ford, M. R. Haas, J. M. Jenkins, D. G. Koch, J. Li, J. J. Lissauer, P. J. MacQueen, C. K. Middour, J. A. Orosz, J. F. Rowe, J. H. Steffen, W. F Welsh, *Science* **2011**, *331*, 562.

[17] W. Wan, J. Gao, X. Yang, *ACS Nano* **2016**, *10*, 10671.

[18] X. Ni, A. V. Kildishev, V. M. Shalaev, *Nat. Commun.* **2013**, *4*, 1.

[19] X. Zhang, M. Theuring, Q. Song, W. Mao, M. Begliarbekov, S Strauf, *Nano Lett.* **2011**, *11*, 2715.

[20] C. Genet, T. W. Ebbesen. *Nanoscience and Technology: A Collection of Reviews from Nature Journals*, World Scientific Publishing Co., Singapore **2009**, pp. 205–212.

[21] Q. Chen, D. R. S. Cumming, *Opt. Express* **2010**, *18*, 14056.

[22] D. Inoue, A. Miura, T. Nomura, H. Fujikawa, K. Sato, N. Ikeda, D. Tsuya, Y. Sugimoto, Y Koide, *Appl. Phys. Lett.* **2011**, *98*.

[23] T. Xu, Y. K. Wu, X. Luo, L. J. Guo, *Nat. Commun.* **2010**, *1*, 59.

[24] Y. K. R. Wu, A. E. Hollowell, C. Zhang, L. Jay Guo, *Sci. Rep.* **2013**, *3*, 1.

[25] B. Zeng, Y. Gao, F. J. Bartoli, *Sci. Rep.* **2013**, *3*, 1.

[26] R. Rajasekharan, E. Balaur, A. Minovich, S. Collins, T. D. James, A. Djalalian-Assl, K. Ganesan, S. Tomljenovic-Hanic, S. Kandasamy, E. Skafidas, D. N. Neshev, P. Mulvaney, A. Roberts, S Prawer, *Sci. Rep.* **2014**, *4*, 1.

[27] T. Li, S. M. Wang, J. X. Cao, H. Liu, S. N. Zhu, *Appl. Phys. Lett.* **2010**, *97*.

[28] V. R. Shrestha, S. S. Lee, E. S. Kim, D. Y. Choi, *Nano Lett.* **2014**, *14*, 6672.

[29] X. Zhu, C. Vannahme, E. Højlund-Nielsen, N. A. Mortensen, A. Kristensen, *Nat. Nanotechnol.* **2016**, *11*, 325.

[30] C. Yang, W. Shen, J. Zhou, X. Fang, D. Zhao, X. Zhang, C. Ji, B. Fang, Y. Zhang, X. Liu, L. J Guo, *Adv. Opt. Mater.* **2016**, *4*, 1981.

[31] M. Elbahri, M. Abdelaziz, S. Homaeigohar, A. Elsharawy, M. Keshavarz Hedayati, C. Röder, M. El Haj Assad, R Abdelaziz, *Adv. Mater.* **2018**, *30*, 1704442.

[32] W. Heller, *J. Colloid Interface Sci.* **1971**, *35*, 181.

[33] C. G. Poulton, L. C. Botten, R. C. McPhedran, N. A. Nicorovici, A. B. Movchan, *SIAM J. Appl. Math.* **2001**, *61*, 1706.

[34] M. A. Biot, *J. Acoust. Soc. Am.* **1968**, *44*, 1616.

[35] P. Sciau, in *The Delivery of Nanoparticles*, Vol. *115*, InTech Open Access Publisher **2012**, pp. 525–540.

**ADVANCED
SCIENCE NEWS**

www.advancedsciencenews.com

**ADVANCED
PHOTONICS
RESEARCH**
Open Access

www.adpr-journal.com

[36] M. Elbahri, M. K. Hedayati, S. Homaeigohar, M. Abdelaziz, *Front. Nanosci.* **2020**, *15*, 185.

[37] M. Elbahri, A. U. Zillohu, B. Gothe, M. K. Hedayati, R. Abdelaziz, H. J. El-Khozondar, M. Bawa'aneh, M. Abdelaziz, A. Lavrinenko, S. Zhukovsky, S Homaeigohar, *Light Sci. Appl.* **2015**, *4*, e316.

[38] M. Abdelaziz, S. Homaeigohar, M. K. Hedayati, M. A. Assad, M. Elbahri, *Adv. Opt. Mater.* **2019**, *7*, 1900737.

[39] M. Abdelaziz, R. Abdelaziz, S. Homaeigohar, E. S. Zarie, M. Z. Yetik, L. P. Sederholm, T. M. Liljeström, N. Peippo, S. Pflesser, A. B. Soliman, M Elbahri, *Adv. Mater. Interfaces* **2019**, *6*, 1801610.

[40] S. Homaeigohar, M. Elbahri, *Adv. Opt. Mater.* **2019**, *7*, 1801101.

[41] M. Keshavarz Hedayati, M. Elbahri, *Plasmonics* **2017**, *12*, 1463.

[42] T. Yahagi, M. Degawa, Y. Seino, T. Matsushima, M Nagao, *Cancer Lett.* **1975**, *1*, 91.

[43] H. Ali, *Water, Air, Soil Pollut.* **2010**, *213*, 251.

[44] C. A. Martínez-Huitle, S. Ferro, *Chem. Soc. Rev.* **2006**, *35*, 1324.

[45] L. Monico, G. Van der Snickt, K. Janssens, W. De Nolf, C. Miliani, J. Verbeeck, H. Tian, H. Tan, J. Dik, M. Radepont, M Cotte, *Anal. Chem.* **2011**, *83*, 1214.

[46] B. Yang, H. Cheng, S. Chen, J. Tian, *Mater. Chem. Front.* **2019**, *3*, 750.

[47] The All-New Lexus LC Structural Blue Edition | Lexus Europe, https://www.lexus.eu/discover-lexus/lexus-news/lc-structural-blue#gallery (accessed: February 2021).

[48] E. Laux, C. Genet, T. Skauli, T. W. Ebbesen, *Nat. Photonics* **2008**, *2*, 161.

[49] W. Cai, U. K. Chettiar, H. K. Yuan, V. C. de Silva, A. V. Kildishev, V. P. Drachev, V. M Shalaev, *Opt. Express* **2007**, *15*, 3333.

[50] G. Si, Y. Zhao, H. Liu, S. Teo, M. Zhang, T. Jun Huang, A. J. Danner, J. Teng, *Appl. Phys. Lett.* **2011**, *99*, 033105.

[51] Y. J. Liu, G. Y. Si, E. S. P. Leong, B. Wang, A. J. Danner, X. C. Yuan, J. H Teng, *Appl. Phys. A Mater. Sci. Process.* **2012**, *107*, 49.

[52] G. Si, Y. Zhao, J. Lv, M. Lu, F. Wang, H. Liu, N. Xiang, T. J. Huang, A. J. Danner, J. Teng, Y. J Liu, *Nanoscale* **2013**, *5*, 6243.

[53] Y. Gu, L. Zhang, J. K. W. Yang, S. P. Yeo, C. W. Qiu, *Nanoscale* **2015**, *7*, 6409.

[54] T. Ellenbogen, K. Seo, K. B. Crozier, *Nano Lett.* **2012**, *12*, 1026.

[55] C. Saeidi, D. van der Weide, *Opt. Express* **2014**, *22*, 12499.

[56] J. Do, M. Fedoruk, F. Jäckel, J. Feldmann, *Nano Lett.* **2013**, *13*, 4164.

[57] J. Olson, A. Manjavacas, T. Basu, D. Huang, A. E. Schlather, B. Zheng, N. J. Halas, P. Nordlander, S Link, *ACS Nano* **2016**, *10*, 1108.

[58] W. T. Chen, K. Y. Yang, C. M. Wang, Y. W. Huang, G. Sun, I. D. Chiang, C. Y. Liao, W. L. Hsu, H. T. Lin, S. Sun, L. Zhou, A. Q. Liu, D. P. Tsai, *Nano Lett.* **2014**, *14*, 225.

[59] L. Huang, X. Chen, H. Mühlenbernd, H. Zhang, S. Chen, B. Bai, Q. Tan, G. Jin, K. Cheah, C. Qiu, J. Li, T. Zentgraf, S. Zhang, *Nat. Commun.* **2013**, *4*, 2808.

[60] S. Zou, G. C. Schatz, *Nanotechnology* **2006**, *17*, 2813.

[61] V. A. Markel, A. K. Sarychev, *Phys. Rev. B* **2007**, *75*.

[62] B. Auguié, W. L. Barnes, *Phys. Rev. Lett.* **2008**, *101*, 143902.

[63] C. Zhou, M. Keshavarz Hedayati, X. Zhu, F. Nielsen, U. Levy, A. Kristensen, *ACS Sens.* **2018**, *3*, 784.

[64] Z. Yang, Y. Zhou, Y. Chen, Y. Wang, P. Dai, Z. Zhang, H. Duan, *Adv. Opt. Mater.* **2016**, *4*, 1196.

[65] H. Deng, Z. Li, L. Stan, D. Rosenmann, D. Czaplewski, J. Gao, X. Yang, *Opt. Lett.* **2015**, *40*, 2592.

[66] P. Mao, C. Liu, F. Song, M. Han, S. A. Maier, S. Zhang, *Nat. Commun.* **2020**, *11*, 1538.

[67] Z. Yang, Y. Chen, Y. Zhou, Y. Wang, P. Dai, X. Zhu, H. Duan, *Adv. Opt. Mater.* **2017**, *5*, 1700029.

[68] H. Jiang, S. Alan, H. Shahbazbegian, J. N. Patel, B. Kaminska, *ACS Nano* **2016**, *10*, 10544.

[69] K. Kumar, H. Duan, R. S. Hegde, S. C. Koh, J. N. Wei, J. K Yang, *Nat. Nanotechnol.* **2012**, *7*, 557.

[70] R. Mudachathi, T. Tanaka, *Sci. Rep.* **2017**, *7*, 1.

[71] M. Rezaei, H. Jiang, B. Kaminska, *Nanotechnology* **2016**, *27*, 085301.

[72] J. Xue, Z. K. Zhou, Z. Wei, R. Su, J. Lai, J. Li, C. Li, T. Zhang, X. H. Wang, *Nat. Commun.* **2015**, *6*, 1.

[73] H. Wang, X. Wang, C. Yan, H. Zhao, J. Zhang, C. Santschi, O. J. F. Martin, *ACS Nano* **2017**, *11*, 4419.

[74] M. Miyata, H. Hatada, J. Takahara, *Nano Lett.* **2016**, *16*, 3166.

[75] S. J. Tan, L. Zhang, D. Zhu, X. M. Goh, Y. M. Wang, K. Kumar, C. W. Qiu, J. K Yang, *Nano Lett.* **2014**, *14*, 4023.

[76] G. Wang, X. Chen, S. Liu, C. Wong, S. Chu, *ACS Nano* **2016**, *10*, 1788.

[77] X. Duan, S. Kamin, N. Liu, *Nat. Commun.* **2017**, *8*, 1.

[78] A. U. Zillohu, R. Abdelaziz, S. Homaeigohar, I. Krasnov, M. Müller, T. Strunskus, M. Elbahri, *Sci. Rep.* **2014**, *4*, 1.

[79] M. K. Hedayati, M. Javaheri, A. U. Zillohu, H. J. El-Khozondar, M. S. Bawa'aneh, A. Lavrinenko, F. Faupel, M. Elbahri, *Adv. Opt. Mater.* **2014**, *2*, 705.

[80] M. Großmann, A. Klick, C. Lemke, J. Falke, M. Black, J. Fiutowski, A. J. Goszczak, E. Sobolewska, A. U. Zillohu, M. K. Hedayati, H. Rubahn, F. Faupel, M. Elbahri, M. Bauer, *ACS Photonics* **2015**, *2*, 1327.

[81] Z. Yi, Z. Wang, P. Bai, B. Tang, D. Yuan, L. Jin, L. Shui, R. A. Hayes, G. Zhou, *Prog. Electromagn. Res.*, **2014**, *147*, 95.

[82] P. Camurlu, *RSC Adv.* **2014**, *4*, 55832.

[83] T. Xu, E. C. Walter, A. Agrawal, C. Bohn, J. Velmurugan, W. Zhu, H. J. Lezec, A. A. Talin, *Nat. Commun.* **2016**, *7*, 10479.

[84] B. Comiskey, J. D. Albert, H. Yoshizawa, J. Jacobson, *Nature* **1998**, *394*, 253.

[85] K. Xiong, G. Emilsson, A. Maziz, X. Yang, L. Shao, E. W. Jager, A. B. Dahlin, *Adv. Mater.* **2016**, *28*, 9956.

[86] H. Kim, J. Ge, J. Kim, S. Choi, H. Lee, H. Lee, W. Park, Y. Yin, S. Kwon, *Nat. Photonics* **2009**, *3*, 534.

[87] Y. Kang, J. J. Walish, T. Gorishnyy, E. L. Thomas, *Nat. Mater.* **2007**, *6*, 957.

[88] S. Kim, A. N. Mitropoulos, J. D. Spitzberg, H. Tao, D. L. Kaplan, F. G. Omenetto, *Nat. Photonics* **2012**, *6*, 818.

[89] Y. Y. Li, F. Cunin, J. R. Link, T. Gao, R. E. Betts, S. H. Reiver, V. Chin, S. N. Bhatia, M. J. Sailor, *Science* **2003**, *299*, 2045.

[90] J. Kim, J. Yoon, R. C. Hayward, *Nat. Mater.* **2010**, *9*, 159.

[91] A. K. Yetisen, H. Butt, F. da Cruz Vasconcellos, Y. Montelongo, C. A. B. Davidson, J. Blyth, L. Chan, J. B. Carmody, S. Vignolini, U. Steiner, J. J. Baumberg, T. D. Wilkinson, C. R. Lowe, *Adv. Opt. Mater.* **2014**, *2*, 250.

[92] T. Hayashi, M. Takinoue, H. Onoe, *presented at 20th Int. Conf. Solid-State Sensors, Actuators Microsystems Eurosensors XXXIII, Transducers 2019 Eurosensors XXXIII*, IEEE **2019**, pp. 582–585.

[93] J. Deng, S. Chen, J. Chen, H. Ding, D. Deng, Z. Xie, *ACS Appl. Mater. Interfaces* **2018**, *10*, 34611.

[94] T. H. Park, S. Yu, S. H. Cho, H. S. Kang, Y. Kim, M. J. Kim, H. Eoh, C. Park, B. Jeong, S. W. Lee, D. Y. Ryu, J. Huh, C. Park, *NPG Asia Mater.* **2018**, *10*, 328.

[95] L. Rayleigh, *Phil. Mag.* **1871**.

[96] J. Marra, S. Martin, *Limnol. Oceanogr. Bull.* **2015**, *24*, 97.

[97] H. Fujiwara, *Spectroscopic Ellipsometry: Principles and Applications*, John Wiley & Sons **2007**.

[98] V. Astapenko, *Polariz. Bremsstrahlung Atoms, Plasmas, Nanostruct. Solids* **2013**, *72*, 347.

[99] M. A. Rahman, S. M. K. Vivek, S. H. Kim, J. Y. Byun, *Appl. Surf. Sci.* **2020**, *505*, 144428.

[100] J. Kim, H. Oh, M. Seo, M. Lee, *ACS Photonics* **2019**, *6*, 2342.

[101] J. S. Clausen, E. Højlund-Nielsen, A. B. Christiansen, S. Yazdi, M. Grajower, H. Taha, U. Levy, A. Kristensen, N. A. Mortensen, *Nano Lett.* **2014**, *14*, 4499.

[102] H. G. Schantz, in *IEEE Antennas and Propagation Society*, Vol. *2*, IEEE **2001**, pp. 50–62.

[103] J. D. Jackson, R. F. Fox, *Classical Electrodynamics*, 3rd ed., John Wiley & Sons, New York **1999**.

[104] C. Etrich, S. Fahr, M. K. Hedayati, F. Faupel, M. Elbahri, C. Rockstuhl, *Materials (Basel)*. **2014**, *7*, 727.

[105] L. Y. Yeo, H. C. Chang, P. P. Y. Chan, J. R. Friend, *Small* **2011**, *7*, 12.

[106] A. G. Brolo, *Nat. Photonics* **2012**, *6*, 709.

[107] M. C. Estevez, M. A. Otte, B. Sepulveda, L. M. Lechuga, *Anal. Chim. Acta* **2014**, *806*, 55.

[108] N. Liu, M. Mesch, T. Weiss, M. Hentschel, H. Giessen, *Nano Lett.* **2010**, *10*, 2342.

[109] C. Sönnichsen, B. M. Reinhard, J. Liphardt, A. P. Alivisatos, *Nat. Biotechnol.* **2005**, *23*, 741.

[110] H. Im, H. Shao, Y. I. Park, V. M. Peterson, C. M. Castro, R. Weissleder, H. Lee, *Nat. Biotechnol.* **2014**, *32*, 490.

[111] V. G. Kravets, F. Schedin, R. Jalil, L. Britnell, R. V. Gorbachev, D. Ansell, B. Thackray, K. S. Novoselov, A. K. Geim, A. V. Kabashin, A. N. Grigorenko, *Nat. Mater.* **2013**, *12*, 304.

[112] J. N. Anker, W. P. Hall, O. Lyandres, N. C. Shah, J. Zhao, R. P. Van Duyne, *Nat. Mater.* **2008**, *7*, 442.

[113] A. R. Halpern, Y. Chen, R. M. Corn, D. Kim, *Anal. Chem.* **2011**, *83*, 2801.

[114] A. S. Roberts, A. Pors, O. Albrektsen, S. I. Bozhevolnyi, *Nano Lett.* **2014**, *14*, 783.

[115] J. Wu, Y. Chen, M. Yang, Y. Wang, C. Zhang, M. Yang, J. Sun, M. Xie, X. Jiang, *Anal. Chim. Acta* **2017**, *982*, 138.

[116] J. Begg, *Mater. Des.* **2003**, *24*, 79.

[117] M. K. Hedayati, S. Fahr, C. Etrich, F. Faupel, C. Rockstuhl, M. Elbahri, *Nanoscale* **2014**, *6*, 6037.

[118] M. K. Hedayati, M. Javaherirahim, B. Mozooni, R. Abdelaziz, A. Tavassolizadeh, V. S. Chakravadhanula, V. Zaporojtchenko, T. Strunkus, F. Faupel, M. Elbahri, *Adv. Mater.* **2011**, *23*, 5410.

[119] H. Wang, F. Tam, N. K. Grady, N. J. Halas, *ACS Publ.* **2005**, *109*, 18218.

[120] G. H. Chan, J. Zhao, E. M. Hicks, G. C. Schatz, R. P. Van Duyne, *Nano Lett.* **2007**, *7*, 1947.

[121] A. Henglein, *Chem. Mater.* **1998**, *10*, 444.

[122] M. D. Mcmahon, R. Lopez, H. M. Meyer, L. C. Feldman, R. F. Haglund, *Appl. Phys. B* **2005**, *80*, 915.

[123] P. M. Schwab, C. Moosmann, K. Dopf, H.-J. Eisler, *Opt. Express* **2015**, *23*, 26533.

[124] M. W. Knight, N. S. King, L. Liu, H. O. Everitt, P. Nordlander, N. J. Halas, *ACS Nano* **2014**, *8*, 834.

[125] J. Zi, X. Yu, Y. Li, X. Hu, C. Xu, X. Wang, X. Liu, R. Fu, *Proc. Natl. Acad. Sci. USA* **2003**, *100*, 12576.

[126] P. Vukusic, J. R. Sambles, *Nature* **2003**, *424*, 852.

[127] C. I. Aguirre, E. Reguera, A. Stein, *Adv. Funct. Mater.* **2010**, *20*, 2565.

[128] Y. Takeoka, *J. Mater. Chem.* **2012**, *22*, 23299.

[129] L. Zhu, J. Kapraun, J. Ferrara, C. J. Chang-Hasnain, *Optica* **2015**, *2*, 255.

[130] H. Park, Y. Dan, K. Seo, Y. J. Yu, P. K. Duane, M. Wober, K. B. Crozier, *Nano Lett.* **2014**, *14*, 1804.

[131] M. Bonifazi, V. Mazzone, N. Li, Y. Tian, A. Fratalocchi, *Adv. Opt. Mater.* **2020**, *8*, 1900849.

[132] P. Kang, S. O. Ogunbo, D. Erickson, *Langmuir* **2011**, *27*, 9676.

[133] H. Fudouzi, Y. Xia, *Adv. Mater.* **2003**, *15*, 892.

[134] Y. Yang, Y. Pan, P. Guo, *Appl. Surf. Sci.* **2017**, *402*, 400.

[135] F. Cheng, J. Gao, S. T. Luk, X. Yang, *Sci. Rep.* **2015**, *5*, 1.

[136] J. Zheng, Z.-C. Ye, Z.-M. Sheng, *Opt. Mater. Express* **2016**, *6*, 381.

[137] L. Wen, Q. Chen, X. Hu, H. Wang, L. Jin, Q. Su, *ACS Nano* **2016**, *10*, 11076.

Adel Assad obtained his B.Sc. degree in sustainable and renewable energy from the University of Sharjah, UAE, and his M.Sc. degree with Honors in materials engineering majoring in functional materials and minoring in fiber and polymers engineering from Aalto University, Finland. He is currently a doctorate candidate under the supervision of Prof. Mady Elbahri in the Nanochemistry and Nanoengineering group at Aalto University, Finland. His interests lie in the areas of optics, thin films, plasmonics and polarizonics, and solar energy harvesting.

Shahin Homaeigohar is an assistant professor of biomedical engineering at the University of Dundee, UK. He is a Baxter Fellow and a former Marie-Skłodowska Curie Postdoc Fellow. Receiving a Helmholtz-DAAD Ph.D. Fellowship, he did his Ph.D. research on nanostructured polymeric membranes and graduated in materials engineering in 2011 from the University of Kiel, Germany. He has worked internationally and done impactful research at several universities from Iran, Germany, Finland, Taiwan, to the United Kingdom, reflected in 48 publications and recognized by multiple awards. His research interest includes polymeric nanomaterials for water treatment, wound dressing, and tissue engineering.

ADVANCED
SCIENCE NEWS

www.advancedsciencenews.com

ADVANCED
PHOTONICS
RESEARCH
Open Access

www.adpr-journal.com

Mady Elbahri obtained his B.Sc. from Cairo University, Egypt, and his M.Sc. from the Technical University of Clausthal, Germany. He received his Ph.D. "with highest honors" in the field of nanotechnology and his Habilitation in material science from Christian-Albrechts-University Kiel, Germany. Elbahri is known as the founder of the Leidenfrost chemistry and the polarizonic phenomenon, which have been recognized by several awards including the DGM award of 2021 from the German Society of Material Science. From disorder nanophotonics to functional macroscopic architectures deployed in energy, environment, and life science is the sustainable mission of the Nanochemistry and Nanoengineering group.